Max-Planck-Institut
für Meteorologie

REPORT No. 211

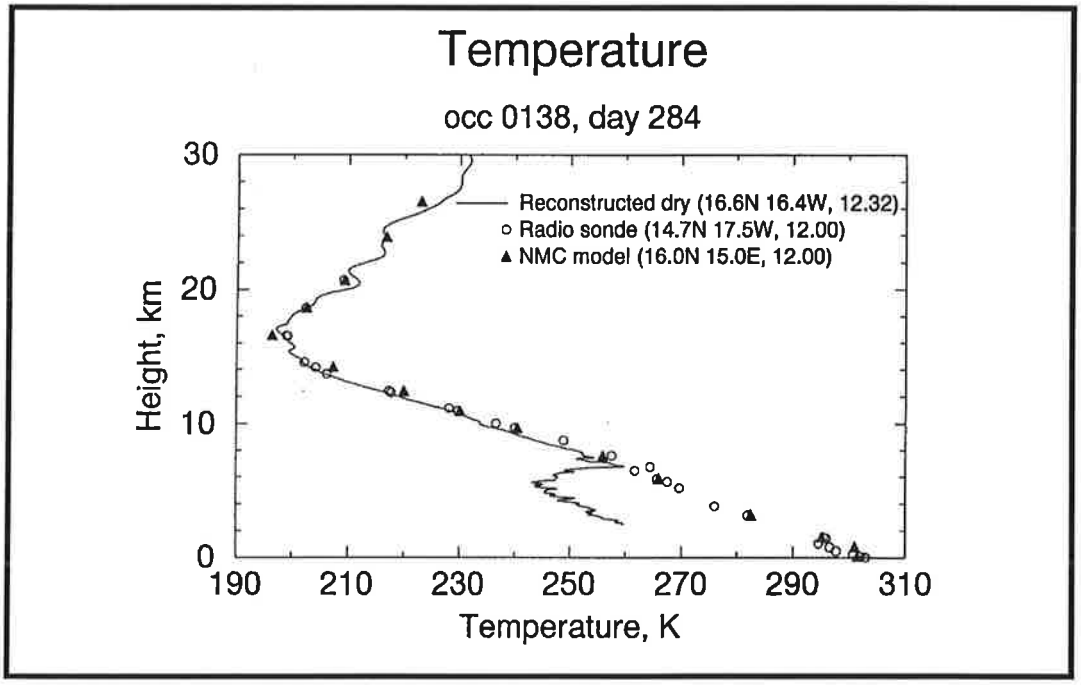

ADVANCED ALGORITHMS OF INVERSION OF GPS/MET SATELLITE DATA AND THEIR APPLICATION TO RECONSTRUCTION OF TEMPERATURE AND HUMIDITY

by

M. E. Gorbunov • A. S. Gurvich • L. Bengtsson

HAMBURG, August 1996

ISSN 0937 – 1060

AUTHORS:

M. E. Gorbunov,
A. S. Gurvich

Russian Academy of Sciences
Moscow
Russia

L. Bengtsson

Max-Planck-Institute for Meteorology
Hamburg
F. R. Germany

MAX-PLANCK-INSTITUT
FÜR METEOROLOGIE
BUNDESSTRASSE 55
D-20146 HAMBURG
F.R. GERMANY

Tel.: +49 - (0)40 - 411 73 - 0
Telefax: +49 - (0)40 - 411 73 - 298
E-Mail: <name>@dkrz.de

Advanced Algorithms of Inversion of GPS/MET Satellite Data and their Application to Reconstruction of Temperature and Humidity

M. E. Gorbunov * • A. S. Gurvich * • L. Bengtsson

Max-Planck-Institute for Meteorology
Bundesstraße 55
D-20146 Hamburg
F.R. Germany

ISSN 0937 - 1060

* Russian Academy of Sciences, Moscow, Russia

Max-Planck-Institute for Meteorology

Report

ADVANCED ALGORITHMS OF INVERSION OF GPS/MET SATELLITE DATA AND THEIR APPLICATION TO RECONSTRUCTION OF TEMPERATURE AND HUMIDITY

by:

M. E. Gorbunov, A. S. Gurvich, and L. Bengtsson

Abstract

In this report, we present the results of elaboration of methods of inversion of the GPS/MET satellite data taking diffraction and multipath effects into account. The first results of the GPS/MET program of sounding of the Earth's atmosphere by means of a Low Earth Orbit satellite implemented with a GPS receiver, indicated that in the lower troposphere, the phase and amplitude of the signal received undergo strong oscillations. This effect is a consequence of multipath propagation resulting from complicated structure of the atmospheric refractivity in the tropical regions. We propose a method of processing the phase measurements, based on the theory of diffraction. The method was tested in processing GPS/MET radio soundings. Comparison of the reconstructed profiles of the temperature and humidity with those derived from the radiosonde measurements extracted from the NMC Global Atmospheric Circulation Model, indicates validity of the method proposed. An approach to the nudging assimilation of the GPS/MET refractometric data is proposed.

Introduction

The first results of the GPS/MET program of radio sounding of the Earth atmosphere (*Ware et al.*, 1996) indicate that the main difficulties of processing of the phase measurements performed by a Low Earth Orbit (LEO) satellite implemented with a GPS receiver, arise in the lowest part of radio occultations. These difficulties are connected with decreasing of the amplitude of the signal received due to the refractive attenuation which impedes tracking of the signal and worsens the signal/noise ratio. But the necessity of careful tracking of the signal increases significantly in the lower troposphere, especially in the tropical regions, because complicated structure of the atmospheric refractivity in these regions results in multipath propagation, i.e. the situation when several rays arrive at the receiver. The analysis of the GPS/MET radio occultations indicates that this situation is a rule rather then an exception.

Processing of the radio occultation phase measurements is usually based on the concepts of the geometrical optics, such as ray and eikonal (optical path), which allows the refraction angle to be defined as the bending angle of a ray. Measurements of the bending angle are based on calculation of the spatial gradient of the phase of the electromagnetic wave, which is connected with the slope of the phase front and therefore with the direction of a ray which is normal with respect to the phase front. In the case we only have one ray coming to the receiver, we can calculate the Doppler shift of the frequency of the signal received by means of differentiation of the phase with respect to the time, and the Doppler shift can be recalculated to the ray incident angle (*Gorbunov and Sokolovsky*, 1993). Knowledge of the ray incident angle allows the ray impact parameter and the refraction angle to be calculated, using Snell's law. Collecting all the calculated refraction angles with the corresponding impact parameters for a radio occultation, we get a vertical profile of the refraction angle which is used in the inversion algorithms.

Application of this algorithm to real phase data is not straightforward since the measurements contain high frequency noise. Due to the fact that both the impact parameters and the refraction angles are calculated from the derivative of the phase simultaneously, which means that vertical profiles of the refraction angle are derived from the phase by means of a significantly non-linear operation, it follows that the dependence of the refraction angle on the impact parameter is ambiguous (*Gorbunov and Sokolovsky*, 1993). Thus filtering of the phase measurements is necessary.

In the case of interpretation of the phase measurements in a multi-path area, the following difficulties occur:

(i) The calculated spatial gradient of the phase cannot be used for the calculation of the ray direction any longer, due to the fact that the field is a sum of interfering rays with different directions.

(ii) Due to diffraction effects, in some regions, the field cannot be represented as a sum of geometric optical rays.

The general structure of the electromagnetic field while sounding the Earth's atmosphere may be described as follows:

(i) The incident wave from the source is close to a spherical wave.

(ii) The field inside the atmosphere is perturbed by the atmospheric inhomogeneities, but diffraction effects are not yet significant.

(iii) The field after passing through the atmosphere, has multi-path areas where diffraction effects become significant. But even in single ray areas, the diffraction effects will result in a worse spatial resolution which will be limited by the size of the Fresnel zone.

Oscillation of the phase measured due to interference of different rays will also result in ambiguities in vertical profiles of the refraction. Filtering of the phase data can indeed avoid them, but unlike the case of the ambiguities due to the measurement noise, it can only be looked at as an heuristic algorithm of deriving of the refraction angle from the phase measurements.

Another argument in favor of a more accurate algorithm of processing of the radio occultation data is delivered by the fact that filtering eradicates all the information about the fine structure of the atmospheric refractivity in the lower troposphere, but this structure can also be of interest.

In this report, we propose an algorithm for the processing of the radio occultation data based on the theory of diffraction. The basic idea of the algorithm consists using amplitude and phase measurements, i.e. the measurements of the complex amplitude of the electromagnetic field on a satellite orbit, which allows us to calculate the electro-magnetic field in the vertical plane of a radio occultation, i.e. to solve the inverse problem of diffraction. It allows us to transfer from the region of observation to another region located closer to the atmosphere, where the multipath effects are weaker or do not exist, and thus we can "disentangle" the structure of the field received. The recalculation of the electromagnetic field is based on the Helmholtz equation in the vacuum and automatically takes the diffraction effects into account.

In the first part of the report, we perform a numerical simulation based on the thin screen model, in order to investigate the diffraction effects and to compare the geometric optical field with that calculated on the basis of the diffraction theory in a multipath region. This solution of the direct problem of diffraction is then used as the initial data for solution of the inverse problem of diffraction, consisting in reconstruction of the phase screen from the complex field in the observation plane. Thus performed simulation, according to the "closed" scheme, allows the algorithm of solution of the inverse problem to be validated.

In the second part, the algorithm of recalculation of the complex field (diffraction correction) is applied to the real GPS/MET measurements. The recalculated field is used as the input data for an algorithm of processing of the phase measurements based on the geometrical optics, and the profiles of refraction derived, are inverted in the standard way. Thus reconstructed profiles of the temperature and humidity are compared to those derived from the radiosonde measurements and data extracted from the NMC global operational forecasting model.

In the third part, we describe a direct model of refraction and propose an approach to the nudging assimilation of the refractometric data. For a real radio occultation and

corresponding fields from the ECMWF model, we calculate the differences of the model and reconstructed temperature and humidity. Using them, we give an example of calculation of the non-physical terms in the model dynamic equations.

1. DIRECT AND INVERSE PROBLEMS OF DIFFRACTION

In this chapter, we discuss the direct and inverse problems of diffraction, the solution of which constitutes the basis of our algorithm of diffraction correction of the GPS/MET data. The direct problem of diffraction consists in calculation of the wave field in space from its values specified on a given source surface. In our numerical simulation, we used the thin screen model of the atmospheric inhomogeneities, the boundary conditions being specified on the thin screen plane. The inverse problem of diffraction consists in finding the field on the source surface from its observed values on an observation surface.

Two series of numerical simulations were performed. In the first one, the field calculated in the diffraction theory was compared to that given by the geometric optical approximation. The geometry of the source and observation plane was chosen to coincide with that of the GPS/LEO observations. The basic point of the numerical simulation was calculation of the wave field in a multi-path area and in the vicinity of a caustic, where the basic difficulties of interpretation of the phase measurements occur. Caustic is defined as a surfaces tangent to a manifold of rays, where the geometrical optics predicts an infinite amplitude due to focusing.

In the second numerical simulation, the thin screen was reconstructed from the observed wave field. The algorithm of solution of the inverse problem of diffraction, used in that simulation, constitutes the kernel of the diffraction correction based on recalculation of electromagnetic field in the observation plane to that in an auxiliary plane located closer to the atmosphere. The numerical simulation performed, allowed the methods of diffraction correction and of data processing to be validated.

1.1. Basic equations of diffraction theory and their solution

The complex amplitude u of the electro-magnetic field in vacuum satisfies the Helmholtz equation:

$$\Delta u + k^2 u = 0 \tag{1.1.1}$$

where $k = \dfrac{2\pi}{\lambda}$ is the wave vector, λ is the wave length.

We shall consider this equation in 2D case which corresponds to consideration of the electro-magnetic field in the radio occultation plane under the assumption that variations of the field in the lateral direction are smooth enough. That can be substantiated by the estimation of the lateral size of the Fresnel zone which is $(L\lambda)^{1/2}$ where L is the distance from the receiver to the ray perigee point. For the GPS/MET observations, L is equal to 3000 km, and λ is about 20 cm which results in the size of the Fresnel zone in the lateral direction about 1 km. This value is significantly smaller than the characteristic horizontal scale of the atmospheric inhomogeneities, and thus it allows us to neglect the diffraction effects when considering the lateral structure of the field.

The vertical size of the Fresnel zone is affected by the regular refraction and is estimated as $(L\lambda)^{1/2}\left(1-L\frac{d\epsilon}{dp}\right)^{-1/2}$ (*Melbourne et al.*, 1994), where ϵ is the refraction angle, and p is the impact parameter. This value is about 0.2 km in the lower troposphere and increases up to 1 km at a height of 20 km. The vertical size of the Fresnel zone is thus comparable with the characteristic vertical scale of the atmospheric inhomogeneities, and consideration of the vertical structure of the electro-magnetic field must involve account of the diffraction effects.

The Green function of the 2D Helmholtz equation and its large argument expansion are given by the formula (*Vladimirov*, 1988; *Weng Cho Chew*, 1994):

$$G(r)=\frac{1}{4i}H_0^{(1)}(kr)\approx\frac{1}{4i}\left(\frac{2}{\pi kr}\right)^{1/2}\exp(ikr-i\pi/4) \tag{1.1.2}$$

where $H_0^{(1)}(kr)$ is the Hankel function of the 1st kind and 0th order, $r=|x|$ is the distance from the origin of the coordinate system to a point x, and $x=(x_1,x_2)$ is the coordinate vector in the plane in consideration.

Given a closed curve S and the values u_0 of the complex field u at the curve, the solution of the external boundary problem for the Helmholtz equation is represented in the form of the double-layer potential (*Vladimirov*, 1988):

$$u(x)=\frac{\pi i}{2}\int_S\nu(y)\frac{\partial}{\partial n_y}H_0^{(1)}(k|x-y|)dS_y \tag{1.1.3}$$

where n_y is the vector of the external normal of the curve S at a point y, $\frac{\partial}{\partial n_y}$ is the derivative in the direction of the external normal with respect to the variable y, and the potential density $\nu(y)$ is the solution of the following Fredholm integral equation of the second kind on the curve S:

$$u_0(x)=\pi\nu(x)+\frac{\pi i}{2}\int_S\nu(y)\frac{\partial}{\partial n_y}H_0^{(1)}(k|x-y|)dS_y,\qquad x\in S \tag{1.1.4}$$

If S is a straight line, then the integral term in this equation vanishes, because n_y is perpendicular to S and $\frac{\partial}{\partial n_y}|x-y|=0$. In this case, the solution of the boundary problem is expressed in the form:

$$u(x)=\frac{i}{2}\int_S u_0(y)\frac{\partial}{\partial n_y}H_0^{(1)}(k|x-y|)dS_y \tag{1.1.5}$$

Using the large argument expansion of the Green function and neglecting the derivative of the slowly changing factor $\left(\frac{2}{\pi kr}\right)^{1/2}$, we arrive at the following approximate formula:

$$u(x) = \left(\frac{k}{2\pi}\right)^{1/2} \int_S u_0(y) \cos\varphi_{xy} \frac{\exp(ik|x-y| - i\pi/4)}{|x-y|^{1/2}} dS_y \tag{1.1.6}$$

where φ_{xy} is the angle between the normal n_y and the vector $x-y$. This solution describes the waves propagating in the direction from the curve S. For the waves arriving at the curve S, we have a similar formula:

$$u(x) = \left(\frac{k}{2\pi}\right)^{1/2} \int_S u_0(y) \cos\varphi_{xy} \frac{\exp(-ik|x-y| + i\pi/4)}{|x-y|^{1/2}} dS_y \tag{1.1.7}$$

These two formulae may be looked at as two reciprocally inverse transforms, the former calculating the field in the observation plane from that in the source plane, the latter reconstructing the field in the source plane from its observations, the curve S corresponding to the source plane in formula (1.1.6) and to the observation plane in formula (1.1.7).

1.2. Basic equations of geometrical optics and their solution

A widely used approximation for solution of the Helmholtz equation in an inhomogeneous media is the geometrical optics (short wave or WKB approximation (*Weng Cho Chew*, 1994)). Let us write the Helmholtz equation for an arbitrary media with the refraction index $n(x)$:

$$\Delta u + k^2 n^2 u = 0 \tag{1.2.1}$$

The complex field u may be represented as $A\exp(ik\Phi)$. For large values of k, the amplitude A may be expanded into the series with respect to inverse powers of k:

$$A = \sum_{j=0}^{\infty} \frac{A_j}{k^j} \tag{1.2.2}$$

Substituting this representation for u into equation (1.2.1) and collecting terms with the same powers of k, we arrive at the basic equations of the geometrical optics (*Kravtsov and Orlov*, 1990; *Vaganov and Katsenelenbaum*, 1982):

$$(\nabla\Phi)^2 = n^2 \tag{1.2.3a}$$

$$\nabla(A_0^2 \nabla\Phi) = 0 \tag{1.2.3b}$$

The former equation is referred to as the eikonal equation, and can be solved using the method of characteristic equation. The equation for the characteristic curves of the eikonal equation in the Cartesian coordinates is

$$\frac{dx_i}{2p_i} = \frac{dp_i}{2n\partial n/dx_i} = \frac{d\Phi}{2p^2} = \frac{d\tau}{2} \tag{1.2.4}$$

where $p = \nabla\Phi$, and τ is the curve parameter (the factor of $1/2$ at $d\tau$ is introduced for convenience). Thus we see, that the characteristic curves are tangent to the vector $\nabla\Phi$, i.e. they are the rays. Using the identity $p^2 = n^2$ (the eikonal equation), we may write the equation for the rays as follows:

$$\frac{d^2x}{d\tau^2} = n\nabla n \tag{1.2.5}$$

The parameter τ is related to the ray arc length by the identity $d\tau = ds/\mathrm{n}$. This equation can only be used in the Cartesian coordinates.

Equation (1.2.3b) indicates that the vector $A_0^2\nabla\Phi = A_0^2 n\frac{dx}{ds}$ is the flow density of a conserving quantity (energy), being equal to the absolute value nA_0^2 of the vector (the energy density), which is transferred along rays (in the 0-order approximation, no energy exchange between different rays exists). Introducing the cross-section of a ray tube σ, we can write the energy conservation law in the form

$$nA_0^2\sigma = \mathrm{const} \tag{1.2.6}$$

1.3. Thin screen model

In a numerical simulation, we used the thin screen model of the atmospheric inhomogeneities, and calculated the complex field in an observation plane using geometrical optics and diffraction theory.

The thin screen model consists in representation of a 3D inhomogeneous medium, through which the wave propagates, as an infinitely thin layer giving the equivalent phase delay. Usage of that model can be substantiated in the case when diffraction effects are not significant inside the inhomogeneous medium and the structure of the incident wave is not strongly perturbed. Usage of the thin screen model is sensible, for instance, in the problems of description of the statistical characteristics of waves in random media.

In general, its usage may prove questionable. Particularly, it is the case in interpretation of the GPS/MET data, where a high accuracy is required. We must emphasize that the thin screen model is not a part of our algorithm of diffraction correction, and it is only used as the generator of the source field in the numerical simulation.

The thin screen parameters were chosen from the model of the refractivity field represented as the sum of the spherically symmetrical exponential unperturbed refractivity and its Gaussian perturbation:

$$n(h,z) = n_0\left(\sqrt{(a+h)^2+z^2}\right) + \delta n(h,z)$$

$$n_0(r) = N_0\exp\left(-\frac{r-a}{H}\right)$$

$$\delta n(h,z) = \alpha \exp\left(-\frac{(h-h_0)^2}{\Delta h^2} - \frac{z^2}{\Delta z^2}\right) \tag{1.3.1}$$

where h and z are the vertical and horizontal coordinates respectively, the thin screen location corresponding to $z = 0$; a is the Earth's radius, $N_0 = 3 \times 10^{-4}$ is the characteristic value of the refractivity at the Earth's surface. The equivalent optical thickness $\Phi(h)$ of the screen is calculated by means of integration of $n(h,z)$ with respect to z which gives

$$\Phi(h) = \sqrt{2\pi a H} n_0 (a+h) + \alpha\sqrt{\pi}\Delta z \exp\left(-\frac{(h-h_0)^2}{\Delta h^2}\right) \tag{1.3.2}$$

The regular exponential part of the optical thickness is thus a big defocusing lens, while the perturbation is a small focusing one. In the numerical simulations performed, we considered the situations when the observation plane is located in front or in the rear of the area of focusing, which correspond to absence or presence of the multipath propagation respectively. For this purpose, the amplitude α and the characteristic vertical size Δh were varied. The characteristic horizontal size Δz of the perturbation δn and the height h_0 of its location were taken to be 300 km and 2 km respectively.

Calculation of the field in the geometric optical approximation was based on finding rays and summation of the fields corresponding to different rays in the observation plane. The direction of the ray differs from the direction of the normal to the phase screen plane by the angle ϵ (refraction angle) defined by the formula:

$$\epsilon = -\frac{d\Phi}{dh} \tag{1.3.3}$$

If the observation plane is located at a distance L from the phase screen plane, then the ray starting at a height h comes to the point with the vertical coordinate $h - L\epsilon$. The amplitude A of the ray is defined by the following formula which is a consequence of (1.2.6):

$$A = A_0 \left(\frac{\sigma_0}{\sigma}\right)^{1/2} \tag{1.3.4}$$

where A_0 is the ray amplitude at the phase screen which was taken to be unity, σ_0 and σ are the the cross sections of the ray tube at the phase screen and in the vicinity of the observation point respectively.

The phase φ of the ray is equal to

$$\varphi = k\left(\Phi(h) + L\left(1+\epsilon^2\right)^{1/2}\right) + \Delta\varphi \tag{1.3.5}$$

where $\Delta\varphi$ is the phase addition which is 0 for a ray having no points tangent to a caustic, and $-\pi/2$ otherwise (*Kravtsov and Orlov*, 1990; *Weng Cho Chew*, 1994). The complete geometric optical field in an observation point is calculated as the sum of the complex fields corresponding to all the rays coming to the point.

1.4. Numerical simulation of direct and inverse diffraction problems

The comparison of the phases and amplitudes calculated in the geometrical optics and in the diffraction theory in the simplest situation without multipath propagation, is illustrated by Figure 1. The parameter values of the phase screen are $\alpha = 0.5$ N (the N-unit of the refractivity is equal to 10^{-6}), $\Delta h = 0.6$ km. This and further figures represent the accumulated phase calculated by means of scanning of the complex field with summation of change of its phase and adding $\pm 2\pi$ in the points of transfer of the phase from $\pm\pi$ to $\mp\pi$.

The differences between the geometric optical and diffracted fields are scarcely visible, which stays in a good agreement with the fact that the characteristic vertical scale of the perturbation (0.6 km) exceeds the size of the Fresnel zone (0.2 km).

The situation of a perturbation with a vertical scale comparable with the size of the Fresnel zone is represented in Figure 2. The correspondent parameters are $\alpha = 0.05$ N, $\Delta h = 0.15$ km. In this case the geometrical optics predicts a much sharper focusing of the field than it really takes place.

Figures 3 and 4 represent the field in presence of the multipath propagation. In the both cases, the characteristic vertical size of the perturbation Δh is equal to 0.6 km, and its amplitudes α are 2N and 5N respectively. These figures indicate a very good agreement between the geometrical optics and diffraction theory in one-ray and multi-ray areas (for $\alpha = 5$N, the difference of accumulated phases in the multipath area is equal to 2π). Large differences occur on the caustic, where the geometrical optics predicts very sharp spikes of the amplitude due to the focusing, which do not appear in the field calculated in the diffraction theory. It is also the case in the vicinity of the caustic, particularly outside the multipath area, where the diffraction theory gives an oscillating field, while the geometrical optics does not predict any interference there.

Figure 5 shows the results of reconstruction of the phase screen from the field in the observation plane. The errors of the reconstruction of the phase are negligibly small as compared to the characteristic value of the perturbation of the phase screen optical thickness which is about 80 rad.

Figure 6 shows similar results in the case when a noise in the measurements of the field in the observation plane was simulated. The statistical characteristics of the noise were similar to those in the GPS/MET data. The amplitude noise was 5% of its vacuum value, the phase noise was 10 mm (about 0.3 rad). The phase reconstruction error proves to be of the same order, which indicates the stability of the inverse problem of diffraction with respect to a high-frequency noise.

2. ALGORITHMS OF INVERSION OF GPS/MET DATA

In this chapter, we describe an algorithm of inversion of the high precision phase measurements on limb paths, performed by a LEO satellite Microlab-1 implemented with a GPS receiver.

The basic problem here, is that of processing of phase measurements in presence of the multipath propagation occurring in the lower troposphere. The multipath propagation is caused by strong gradients of the refraction index, that are connected with complicated structure of the humidity field. Albeit the regular, approximately exponential decrease of the refraction index with the height may be treated as a negative lens diverging the rays, the irregular perturbations of the structure of the "lens" in the lower troposphere are strong enough to distort the structure of the ray configuration so as to result in their intersection, i.e. multipath propagation. The bigger is the distance from the atmosphere to the observation point, the more probable is the multipath propagation.

The field in a multipath zone may be represented as a sum of the fields corresponding to different interfering intersecting rays. The amplitude and phase of the field will thus undergo strong oscillations. In a one-ray zone, the derivative of the phase along the satellite trajectory is uniquely related to the projection of the wave vector to the trajectory direction. That allows the incident ray angle to be calculated with the ray direction known, the impact parameter and the refraction angle can also be found from Snell's law. But in a multipath zone, this is not the case, since the phase derivative being defined by the interference effect, and no unique value of the ray incident angle for a trajectory point existing.

Our algorithm of processing of the phase measurement is based on the theory of diffraction, which allows the complex field (phase and amplitude) measured on a satellite trajectory to be recalculated for a region where the multipath effects do not exist. This method of recalculation of the field is termed diffraction correction. An example of such recalculation was given in Chapter 1. In the numerical simulation described there, the field in the observation plane where the multipath effects occurred, was used for reconstruction of the field in the plane of the thin screen where no multipath existed.

Another problem is connected for calculation of the Doppler frequency shift from the phase measurements which requires differentiation the dependence of the phase on the time, experimentally measured and thus containing random noise. Our approach to that problem was based on consequent use of the statistical optimization.

In the upper part of the profile, the measurement errors become comparable with the refraction angles. In order to reduce the errors of reconstruction the meteorological fields, we combine the measured refraction profile with that calculated for the CIRA standard atmospheric model. The method of combining of measured and model profiles was also based on statistical optimization.

The general scheme of processing of the GPS/MET satellite data included:

1) Diffraction correction of the measurements in the lower troposphere.

2) Differentiation of the phase with respect to the time giving the Doppler frequency shift, and calculation of the ray impact parameters and refraction angles.

3) Exclusion of the ionospheric input in the refraction angle.

4) Combining of the refraction angle profile derived from the phase measurements with that calculated for the CIRA standard atmospheric model.

5) The Abel inversion of the refraction angle profile and derivation of the temperature and humidity.

2.1. Diffraction correction

Diffraction correction of the GPS-MET data is based on calculation of the wave field in a region nearer to the atmosphere so as to reduce the size of the multi-path area and thus to improve the accuracy of calculation of the refraction angle from the phase measured.

Calculation of the corrected field was based on formula (1.1.7), although the curve on which the field is specified, i.e. the satellite orbit is not a straight line. The strict solution could be represented in a form similar to (1.1.3) and (1.1.4), but the radius of the LEO orbit is very large as compared to the size of the Fresnel zone, so formula (1.1.7) which is written for a straight line, provides a sufficient accuracy.

During an occultation, both GPS and LEO satellite move, and the sounding rays do not lie in the same vertical plane passing through the Earth's center. In order to make the 2D solution applicable to the situation, we transform the data as follows.

For each position of GPS and LEO satellites during an occultation, we introduce the local coordinates z and ξ in the vertical plane defined by three points: GPS and LEO satellite positions and the Earth's center. The straight line from GPS, tangent to the Earth's surface is the z-axis, the origin point of the coordinate system is the point where the line touches the Earth's surface, and the ξ-axis is directed vertically, perpendicularly to the z-axis. For each moment of time, the local (z, ξ) coordinates of the satellites are then treated as applied to the same plane. The relative rotation of the Earth with respect to the configuration described is neglected.

We shall now change the satellite positions so that the GPS satellite should become stationary during the occultation. Introducing the angles ϵ_1 and ϵ_2 between the ray and the straight line connecting the satellites, we can write Snell's law:

$$\epsilon_1 z_1 = \epsilon_2 z_2 = p - a \tag{2.1.1}$$

where z_1 and z_2 are z-coordinates of the satellites, p is the ray impact parameter and a is the local Earth's radius. Then we can write the equation for the full refraction angle $\epsilon = \epsilon_1 + \epsilon_2$:

$$p - a = \frac{z_1 z_2}{z_1 + z_2} \epsilon(p) \tag{2.1.2}$$

This equation indicates that if z_1 and z_2 are changed so that

$$\frac{z_1 z_2}{z_1 + z_2} = \text{const} \tag{2.1.3}$$

then the refraction angle does not change. Using relationship (2.1.3), we can change both GPS and LEO z-coordinates so that the new coordinates of the GPS satellite should be constant.

Using the satellite coordinates thus transformed, we can perform a diffraction transform (1.1.7) so as to calculate the field in the auxiliary plane. We located the plane at $z_0 = 100$ km.

The numerical algorithm for the calculation the diffraction integral was based on analysis of the behavior of the subintegral expression

$$u_0(y) \cos \varphi_{xy} \frac{\exp(-ik \mid x - y \mid + i\pi/4)}{\mid x - y \mid^{1/2}} \tag{2.1.4}$$

where x is the coordinate vector of a point in the auxiliary plane, y is the coordinate vector of a point on the LEO orbit, u_0 is the complex field measured.

The most significant part of the integration area lies in the vicinity of the stationary point of the phase of this expression, which is equal to

$$\varphi = \arg(u_0(y)) - k \mid x - y \mid \tag{2.1.5}$$

For each point x on the auxiliary plane, the corresponding point y on the observation curve was found where the phase φ had the absolute extremum. The integration area was then defined as the area where the difference between the current and extreme values of φ did not exceed some specified value $\Delta\varphi$. The value of $\Delta\varphi = 10\pi$ proved to provide sufficient accuracy of calculation (increasing of this value say to 70π did not yield any remarkable change of the result of calculation). The value of the diffraction integral over the integration area defined above, was corrected with account of its asymptotic behavior.

The field corrected was then available for its usage by inversion algorithms. The correction was only applied to the very low part of occultations where multi-path propagation can occur, because usage of a corrected field in a one-ray region gives results indiscernible from those for an uncorrected field.

2.2. Calculation of the refraction angle profile

The refraction angle can be calculated from the Doppler frequency shift using Snell's law and the fact that the Doppler shift is connected with the projection of the wave vector to the direction of a satellite's speed. The methods of deriving of the refraction angle from the Doppler shift measurements and its ionospheric correction are described, for example, by *Vorob'ev and Krasil'nikova* (1994), so we do not dwell on them here.

The Doppler shift f is the derivative of the phase φ measured. The Microlab-1 satellite data consist of high-precision phase and amplitude measurements along with coordinates

and velocities of the LEO and GPS satellites with the sampling rate being equal to 50 Hz (*UCAR*, 1994). The data contain uncorrelated measurement noise. The noise in the amplitude is about 5% of its vacuum value. For the phase, it constitutes 10 mm. Thus we arrive at the problem of differentiation of an empirical function contaminated with random measurement errors.

Derivation of the Doppler shift was done in two steps. At first, the phase trend $\varphi^{(0)}$ was calculated by means of the spline regression. Differentiation of a spline is reduced to calculation of the derivative of a cubic polynomial. The part $\Delta\varphi$ remaining after subtraction of the trend was differentiated by means of the methods of statistical optimization (*Turchin and Nozik*, 1969; *Ustinov*, 1990). Denoting $f^{(0)} = \frac{d\varphi^{(0)}}{dt}$ and $\Delta f = \frac{d\Delta\varphi}{dt}$, we can write an integral equation for Δf:

$$\int_0^t \Delta f(t')dt' = \Delta\varphi(t) \tag{2.2.1}$$

Specifying the set $\{\tau_j\}$ of the moments of time, at which we need the values of $\Delta f_j = \Delta f(\tau_j)$, and introducing the vector of the measurements $\Delta\varphi_i = \Delta\varphi(t_i)$, we can write equation (2.2.1) in a discretized form:

$$\sum_j K_{ij}\Delta f_j = \Delta\varphi_i \tag{2.2.2}$$

where the kernel matrix K can be derived using, for example, the Simpson approximation for integral (2.2.1).

Given the correlation matrices O and C of the measurement error and of the unknown vector Δf respectively, we can write the most probable value of the solution (accepting the Gaussian statistics both for measurement error and for the unknown vector) in the form:

$$\Delta f = \left(K^T O^{-1} K + C^{-1}\right)^{-1} \left(K^T O^{-1} \Delta\varphi\right) \tag{2.2.3}$$

The correlation matrix of the measurement error was taken to be diagonal. The grid $\{\tau_j\}$ was taken with a step of 0.1 sec, which corresponds to a vertical resolution of 100 m. The correlation matrix of the unknown vector was taken to be triangle with a characteristic scale of the correlation of 2 sec, which corresponds to a vertical correlation scale of 2 km.

2.3. Combining of measured and model refraction profiles

In the highest part of the refraction angle profile, the measurement errors become comparable with the deviations of the refraction angle from its mean statistical value. Thus it is expedient to combine the measured profile of the refraction angle with the model one.

Our method of combining of those profiles of the refraction angle was based on the statistical optimization. The model profile of the refraction angle was calculated for CIRA standard atmospheric model (*Strickland*, 1972).

Let us assume that we have a measured profile $\epsilon(p)$ and a model profile $\epsilon_{CIRA}(p)$ calculated for the same observation geometry. Denoting $\Delta\epsilon_i = \epsilon(p_i) - \epsilon_{CIRA}(p_i)$ the vector of the deviation of the measured refraction angle profile from the model one, we can express its most probable value as follows

$$\widetilde{\Delta\epsilon} = \left(O^{-1} + C^{-1}\right)^{-1} \left(O^{-1}\Delta\epsilon\right) \tag{2.3.1}$$

where O is the correlation matrix of the error and C is the correlation matrix of $\Delta\epsilon$. We shall now assume that both $\Delta\epsilon$ and the measurement error are uncorrelated and represent the mean-square deviation as follows

$$\langle\Delta\epsilon^2(p)\rangle = \beta \exp\left(-\frac{p}{H}\right) + \xi \tag{2.3.2}$$

where the first term represents the true deviation, and ξ is the mean-square measurement error. Then we can write the following formula for the combined refraction angle profile:

$$\widetilde{\epsilon}(p) = \epsilon_{CIRA}(p) + \frac{\beta \exp\left(-\frac{p}{H}\right)}{\beta \exp\left(-\frac{p}{H}\right) + \xi}\Delta\epsilon(p) \tag{2.3.3}$$

The value of ξ was determined from the highest part of the refraction profile, and the values of β and H were found by means of regression.

Formula (2.3.3) provides a smooth transfer from the measured profile of the refraction angle in the region where the measurement errors are relatively small, to the model one in the region where the measurement errors become comparable with the difference of the measured and model profiles.

2.4. Processing of Microlab-1 satellite data

The above algorithms of processing of the phase measurements were combined and applied to the Microlab-1 satellite data to produce vertical profiles of the refraction. Inversion of the refraction was based on the Abel transform giving the vertical profile of the atmospheric refractivity (*Gorbunov and Sokolovsky*, 1993). In the assumption of the dry air, the temperature profile can be derived from the the reconstructed refractivity.

Due to the humidity effect, the temperature reconstructed will indicate a cold bias in the lower troposphere. That effect can be used so as to reconstruct the humidity if the temperature is known independently (*Ware et al.*, 1996).

Figure 7 (above) represents the refraction angle profile derived from the phase measurements for an occultation observed on October 11, 1995 above the point with the coordinates 16.6N 16.4W, and that calculated from the CIRA model for the same occultation geometry. In the upper part of the profile, the measurement error dominates. Absolute values of the refraction angle are plotted, because in the upper part, due to the errors, the refraction angles have somewhere negative values.

Figure 7 (below) represents a comparison of the refraction angle profile derived from the phase measurements and that calculated after the diffraction correction. This comparison indicates that the conspicuous ambiguities in the initial refraction angle profile, arising in the multipath area, can be completely eliminated after correction. Outside the multipath area, both refraction profiles are in a satisfactory agreement with each other.

Figure 8 shows the results of reconstruction of the temperature and water vapor pressure from the refraction angle profile for the same occultation. A comparison is performed with the temperature and water vapor pressure measured by the nearest radiosonde as well as extracted from the NMC model. The temperature reconstructed is the so-called dry temperature, i.e. the temperature is derived from the refractivity as if there were no humidity. The effect of the water vapor is indicated by the cold bias of the reconstructed temperature, which becomes significant below 8 km. At greater heights, the temperature reconstructed is in a good agreement with the measured and modelled one. Reconstruction of the water vapor was performed from the refractivity and the model or radiosonde temperature. It also indicates a good agreement with the measured and model values.

Figures 9 — 12 show several similar examples, which also indicate that the diffraction correction allows the ambiguities in the vertical profile of the refraction angle to be avoided and the small scale structure of the vertical profiles of the refraction angle to be extracted from the phase measurements.

In the plot represented by Figure 12, a very large error of the temperature measured by the radiosonde at a height of 18 km is to be noticed. Another example of another large radiosonde temperature error at a height of 3 km, is given by Figure 13.

Figure 14 illustrates an error of the GPS receiver which is probably connected with a loss of the signal in the multipath zone in the lower troposphere. The lowest part of the reconstructed temperature profile indicates a significant "warm" bias instead of the cold one.

The above examples indicate the necessity of complex processing of different kinds of data, each having its own kinds of random errors.

3. POSSIBILITIES OF DIRECT ASSIMILATION OF SATELLITE REFRACTOMETRIC DATA INTO A NUMERICAL WEATHER PREDICTION MODEL

The most rational way of using the GPS/MET observations consist in assimilating them into a numerical weather prediction model. Two approaches to this problem are (i) 4-dimensional variational data assimilation (4DVDA) (*Le Dimet and Talagrand*, 1986; *Zou et al.*, 1995; *Eyre*, 1994), and (ii) the Newtonian nudging approach (*Anthes*, 1974; *Zou et al.*, 1992). A distinct advantage of the former method is its possibility to assimilate any data sources, while the nudging assimilation technique only allows for assimilation of model-predicted values. However, a disadvantage of the 4DVDA technique is its strong demand of computer resources, presently impeding its usage in operational applications.

In this chapter, we investigate the possibilities of using the nudging technique for assimilation of the GPS/MET observations. Although both the refraction angles and the atmospheric refractivity are no model-predicted variables, it is possible to use them for calculation of the temperature and humidity profiles which already can be assimilated by means of the nudging technique. One of the difficulties which arises thereby, consists in the reconstructed temperature and humidity being complicated functionals on the atmospheric fields rather than their local values. We propose a way of overcoming it by means of calculating of the refraction angle profiles for the model refractivity field with their subsequent inversion. The temperature and humidity reconstructed from the model refraction, are represented through the same functionals on the model fields. The differences of the temperature reconstructed from the real and model refraction, and the same difference for the humidity, multiplied by the corresponding coefficients, can be used as the non-physical nudging terms in the model dynamic equations.

In our numerical calculations, we used a field from the ECMWF model closest in the time to a radio occultation. We calculate the model refraction angle profile for the observation geometry corresponding to that of the radio occultation. Then we compare the model and measured refraction angle profiles and the temperature and humidity reconstructed from them.

The basic themes of this chapter are:

(i) A description of the direct model used for calculation of the refraction from gridded fields of the temperature and humidity at T106 resolution.

(ii) A description of comparison of the temperature and humidity derived from the refraction angles measured with those derived from the model refraction.

3.1. Direct model

The direct model is used for calculation of the dependence of the refraction angle ϵ on the impact parameter p for a given observation geometry. For this purpose, we integrated the ray trajectory equation (1.2.5) by means of the Runge-Kutta method.

Calculation of the refractivity n and its gradient ∇n for an arbitrary point was based on the following interpolation scheme.

The values of the temperature T_{ijk} and relative humidity $q_{\nu,ijk}$ are given for the Gaussian grid of the latitudes φ_j, the homogeneous grid of the longitudes λ_k, and an irregularly spaced grid of heights (full levels) z_{ijk} which is described below. For T106 resolution of the ECHAM3 model, the indexes have the following ranges: i=1..19 for full-level quantities and i=0..19 for half-level quantities, j=1..160, k=1..320.

The values of the pressure corresponding to the i'th half and full levels are calculated by means of the formulas (*DKRZ*, 1994):

$$P_{i+1/2,jk} = A_{i+1/2} + B_{i+1/2} P_{s,jk} \tag{3.1.1}$$

$$P_{ijk} = \frac{1}{2}\left(P_{i+1/2,jk} + P_{i-1/2,jk}\right) \tag{3.1.2}$$

where $P_{s,jk}$ is the surface pressure for the j'th latitude and k'th longitude, $A_{i+1/2}$ and $B_{i+1/2}$ are the vertical coordinate parameters.

Calculation of the geopotential heights was based on the hydrostatic equation and on an interpolation between the half and full levels (*DKRZ*, 1994):

$$\phi_{i+1/2,jk} - \phi_{i-1/2,jk} = -R_d T_{\nu,ijk} \ln\left(\frac{P_{i+1/2,jk}}{P_{i-1/2,jk}}\right)$$

$$\phi_{i_{\max}+1/2,jk} = \phi_{s,jk} \tag{3.1.3}$$

$$\phi_{ijk} = \phi_{i+1/2,jk} + \alpha_{ijk} R_d T_{\nu,ijk} \tag{3.1.4}$$

$$\alpha_{ijk} = \begin{cases} \ln 2, & i = 1 \\ 1 - \dfrac{P_{i-1/2,jk}}{P_{i+1/2,jk} - P_{i-1/2,jk}} \ln\left(\dfrac{P_{i+1/2,jk}}{P_{i-1/2,jk}}\right), & i > 1 \end{cases} \tag{3.1.5}$$

where R_d is the gas constant for the dry air, $T_{\nu,ijk} = T_{ijk}\left(1 + \left(\frac{R_\nu}{R_d} - 1\right) q_{\nu,ijk}\right)$ is the virtual temperature, R_ν is the gas constant for the water vapor, $\phi_{s,jk}$ is the surface geopotential (orography).

Given the temperature, pressure and humidity at a grid point, the corresponding value of the refractivity was calculated by means of the formula (*Bean and Datton*, 1968):

$$n_{ijk} = c_1 \frac{P_{ijk}}{T_{ijk}} + c_2 \frac{P_{w,ijk}}{T_{ijk}^2} \tag{3.1.6}$$

$$P_{w,ijk} = \frac{q_{\nu,ijk} P_{w,ijk}}{\frac{R_d}{R_\nu} + \left(1 - \frac{R_d}{R_\nu}\right) q_{\nu,ijk}} \tag{3.1.7}$$

where $P_{w,ijk}$ is the water vapor pressure, and the constants $c_1 = 7.76 \times 10^{-5}$ K/mbar, c_2=0.37 K^2/mbar.

For relating of the gridded value of the refractivity to a spatial location, we used the geoid model with the semi-axes being equal to 6378.1363 and 6356.7516 km, and the corresponding gravity field distribution $g(z, \varphi, \lambda)$ (*Dragomir et al.*, 1982; *Lambeck*, 1988), where z is the height above the Earth's surface. Calculation of the geometrical heights z_{ijk} was based on the definition of the geopotential height:

$$\phi_{ijk} = \int_0^{z_{ijk}} g(\zeta, \varphi_j, \lambda_k) d\zeta \tag{3.1.8}$$

For every ϕ_{ijk}, this equation was numerically solved for the corresponding z_{ijk}. Thus the gridded field of the refractivity $n_{ijk} = n(z_{ijk}, \varphi_j, \lambda_k)$ was produced.

For a given point in the Cartesian coordinates (x_1, x_2, x_3), the corresponding geodetic coordinates (z, φ, λ) were calculated. Then the refractivity was interpolated by means of the natural cubic splines with respect to the z-coordinate, and linearly with respect to the φ, λ-coordinates. For calculation of the vertical component of the gradient of the refractivity, the derivative of the spline with respect to the z-coordinate was linearly interpolated with respect to the φ, λ-coordinates. The horizontal component of the gradient was neglected.

The gridded refractivity is given in the height range about 0-30 km. But accurate calculation of refraction requires knowledge of the refractivity up to a height of 120 km. In the height range 30-120 km, we used the refractivity calculated from the CIRA model. For providing a smooth transfer from the exponentially extrapolated gridded refractivity n_{ECHAM3} to that from the CIRA model n_{CIRA}, we used the following formula:

$$n(z) = (n_{ECHAM3}(z) - n_{CIRA}(z)) \exp\left(-\frac{(z - z_0)^2}{\Delta z^2}\right) + n_{CIRA}(z), \quad z > z_0 \tag{3.1.9}$$

where z_0=30 km, Δz=5 km.

For calculation of the dependence $\epsilon(p)$, in the vertical plane defined by the Earth's center and the GPS and LEO positions corresponding to the lowest point of the radio occultation, we calculated a range of rays starting at the GPS positions, with initial directions calculated from the values of the impact parameter.

3.2. An approach to nudging assimilation of the GPS/MET data

The nudging assimilation technique consists in complementing of the dynamic equations of the Global Atmospheric Circulation Model with a non-physical term, describing the

measurements to be assimilated. If X is the vector of the atmospheric state, then the dynamic equation for it can be written in the most general form:

$$\frac{dX}{dt} = F(X) \tag{3.2.1}$$

If we have an observation X^o of the components of the vector X, then the modified dynamic equation takes the form (*Anthes*, 1974; *Zou et al.*, 1992):

$$\frac{dX}{dt} = F(X) + G(X^o - X) \tag{3.2.1}$$

where G is the matrix of the nudging coefficients.

From the view point of the requirements of the computational resources, nudging technique is much simpler than the 4DVDA. Its disadvantage consists in the fact that unlike the 4DVDA technique, it is only capable of assimilation of the model-predicted variables. The obvious difficulty in the case of the GPS/MET measurements is that neither refractivity nor refraction are model-predicted variables.

In order to overcome this difficulty, we modify the basic idea of the nudging assimilation as follows. Let us assume that we know measured and modelled refraction profiles $\epsilon(p)$ and $\epsilon_m(p)$ respectively, and local model-predicted vertical profiles of the temperature $T(z)$ and humidity $q(z)$. Refraction profiles allow the vertical profiles of the refractivity $\widetilde{n}(z)$ and $\widetilde{n}_m(z)$ to be reconstructed. Note that these profiles are not local, because they are related to the real and model 3D fields of refractivity respectively, by the operator represented as the composition of the operator of the direct problem and that of the Abel inversion.

Using the profiles of $\widetilde{n}(z)$ and $q(z)$, we can calculate the temperature profile $\widetilde{T}(z)$, and using $\widetilde{n}(z)$ and $T(z)$, we can find the humidity profile $\widetilde{q}(z)$. Similarly, for the profile $\widetilde{n}_m(z)$, we can calculate the profiles $\widetilde{T}_m(z)$ and $\widetilde{q}_m(z)$. The differences $\widetilde{T}(z) - \widetilde{T}_m(z)$ and $\widetilde{q}(z) - \widetilde{q}_m(z)$, multiplied by the appropriate nudging coefficients, can be now used as the non-physical terms in the dynamic equations for the temperature and humidity respectively.

In a numerical computation of the non-physical terms, we used the radio occultation observed at 12.32 UTC on October 11, 1995 (16.6N 16.4W), and the fields from the ECMWF operational numerical weather prediction model, corresponding to 12.00 UTC of the same day.

Figure 15 shows the observed refraction angle profile $\epsilon(p)$ and the calculated one $\epsilon_m(p)$ for the ECMWF operational numerical weather prediction model. Figure 16 represents a comparison of the profiles $\widetilde{T}(z)$ and $\widetilde{T}_m(z)$ (above), $\widetilde{q}(z)$ and $\widetilde{q}_m(z)$ (below). The most significant differences occur in the lowest part of the profiles, in the height range from 2 to 8 km. Note that the T106 resolution in this area ranges from 1 to 1.7 km, which is significantly worse than the resolution achievable for the radio occultation.

Conclusion

In order to estimate the diffractive effects in the GPS/MET phase observation in presence of multipath propagation, we investigated the direct and inverse problems of diffraction. The observation geometry was chosen close to that in the GPS/MET measurements.

A comparison was performed of the diffracted field with that calculated in the geometric optical approximation. The comparison indicated that the geometrical optics provides a satisfactory description of the field in the observation plane except caustics and their vicinities. On a caustic, the geometrical optics predicts a distinct focusing of the field, the amplitude increasing to the infinity, while in the diffraction theory the field on a caustic has not any singularities. In the vicinity of a caustic, geometric optical and diffracted fields also indicate remarkable difference. Particularly outside a multipath area, the diffraction theory predicts interference effects, which is not the case for the geometrical optics.

The agreement between the geometrical optics and diffraction theory indicates a possibility of hardware processing of the field in a multipath area by means of a multichannel receiver.

Using the diffraction theory, we elaborated an algorithm of derivation of the refraction angle profile from the field measurements in a multipath area. The algorithm was based on recalculation of the field measured on a LEO satellite orbit to an area located closer to the Earth's atmosphere, where multipath effects are at least not so strong or do not exist. Using a recalculated field, a refraction angle profile can be found by means of the standard algorithms based on the geometrical optics in assumption of a one-ray field.

The algorithm of solution of the inverse problem of diffraction, or diffraction correction, was tested, using the thin screen model. In a numerical simulation, the field in the thin screen plane was reconstructed from the field in the observation plane. The results of the numerical simulation indicated stability of the algorithm.

The diffraction correction was applied to the GPS/MET satellite measurements performed by Microlab-1 satellite. The standard algorithms of processing of the phase measurement result in ambiguities in the refraction angle profile due to the phase oscillation which are a result of interference of different rays in the multipath area. Diffraction correction allows the ambiguities to be completely avoided and the thin structure of the refraction index field to be reconstructed.

The refraction angle profiles were inverted by means of the Abel inversion giving vertical profiles of the refractivity, and the dry temperature was the reconstructed. The results of reconstruction of the temperature were compared with the radiosonde measurements and the data extracted from the NMC Global Atmospheric Circulation Model. The temperature profiles reconstructed from the GPS/MET measurements proved to be in satisfactory agreement with the model and measured ones in the height range where the humidity is negligible. In the lower troposphere, the reconstructed temperature indicates a cold bias due to the influence of the humidity. This effect can be used for reconstruction of the water vapor pressure, if the temperature profile is independently known. We used the temperature profile measured by the radiosondes as well as those extracted from the NMC model.

The reconstructed profiles of the water vapor pressure proved also to be in a satisfactory agreement with the model and measured ones.

The algorithms of diffraction correction elaborated, can be used in a system of operational processing of the GPS/MET satellite data.

We propose an approach to the nudging assimilation of the refractometric data, consisting in calculation of the refraction for the predicted model fields of temperature and humidity. The difference of the temperature profiles reconstructed from the model and observed refraction, and a similar difference of the humidity profiles are used in the non-physical terms of the dynamic equations. An example was given of calculation of the non-physical terms, based on the real GPS/MET measurements and fields from the ECMWF numerical operational weather prediction model.

Acknowledgments

This work was sponsored by the Max-Planck Society for Advancement of Science and the University Corporation for Atmospheric Researches. The authors are grateful to M. Exner (University Corporation for Atmospheric Researches), and Dr. S. V. Sokolovsky (Institute for Atmospheric Physics, Russian Academy of Sciences) for discussion of the results. The authors are also grateful to M. Stendel and U. Schulzweida (Max-Planck Institute for Meteorology) for help in acquisition of and work with the ECMWF model data.

References

Anthes, R.: Data Assimilation and Initialization of hurricane prediction models; *J. Atmos. Sci., 31*, 702-719, 1974.

Bean, B. R., and E. J. Datton, *Radio Meteorology*, Dover Publ. Inc., New-York, 1968.

Deutsches KlimaRechenZentrum: The ECHAM3 Atmospheric General Circulation Model, *Technical Report No. 6*, Revision 3, Edited by Deutsches Klimarechenzentrum, Modelbetreuungsgruppe, Hamburg, July 1994.

Dragomir, V., D. Ghitau, M. Mihalescu, M. Rotaru, *Theory of the Earth's shape*, Amsterdam - Oxford - New-York, Elsevier Scientific Publishing Company, 694 pp, 1982.

Eyre, J. R.: Assimilation of Radio Occultation Measurements into a Numerical Weather Prediction System; ECMWF Technical Memorandum No.199, 1994.

Gorbunov, M. E., and S. V. Sokolovsky: Remote sensing of refractivity from space for global observations of atmospheric parameters, *Rep. 119*, Max-Planck Institute for Meteorology, Hamburg, 1993.

Kravtsov, Yu. A., Yu. I. Orlov, *Geometrical Optics of Inhomogeneous Media*, Berlin, Springer, 1990, 312 pp.

Lambeck, K., *Geophysical Geodesy: the slow deformation of the Earth*, Oxford, Clarendon press, 1988, 718 pp.

Le Dimet, F. X., and O. Talagrand: Variational Algorithms for Analysis and Assimilation of Meteorological Observations: Theoretical Aspects; *Tellus, 38A*, 97-110, 1986.

Melbourne, W. G., E. S. Davis, C. B. Duncan, G. A. Hajj, K. R. Hardy, E. R. Kursinski, T. K. Meehan, and L. E. Young, The application of spaceborne GPS to atmospheric limb sounding and global change monitoring, *JPL Publ. 94-18*, Jet Propul. Lab., Pasadena, Calif., 1994.

Strickland, A. C. (editor), *CIRA 1972*, Akademie Verlag, Berlin, 1972.

Turchin, V. F., and V. Z. Nozik: Statistical Regularization of the Solution of Incorrectly Posed Problems; *Izv. Acad. Sci. SSSR, Atmos. Oceanic. Phys., Engl. Transl., 5*(1), 14-18, 1969.

UCAR GPS/MET Data Products Available on POCC, 1994; Boulder.

Ustinov, E. A.: To Solution of the Problem of Numerical Differentiation with the Method of Statistical Regularization; *Kosmicheskie Issledovaniya (Cosmic Researches), 28*(4), 545-554, 1990. (In Russian).

Vaganov, R. B., and B. Z. Katsenelenbaum, *Basis of the theory of diffraction*, Moscow, Nauka press, 1982, 272 pp. (In Russian).

Vladimirov, V. S., *Equations of Mathematical Physics*, Moscow, Nauka press, 1988, 512 pp. (In Russian).

Vorob'ev, V. V., and T. G. Krasil'nikova: Estimation of the Accuracy of the Atmospheric Refractive Index Recovery from Doppler Shift Measurements at Frequencies Used in the NAVSTAR System; *Izv. Acad. Sci. SSSR, Atmos. Oceanic. Phys., Engl. Transl., 29*(5), 602-609, 1994.

Ware, R., M. Exner, D. Feng, M. Gorbunov, K. Hardy, D. Herman, Y. Kuo, T. Meehan, W. Melbourne, C. Rocken, W. Schreiner, S. Sokolovsky, F. Solheim, X. Zou, R. Anthes, S. Businger, and K. Trenberth: GPS Sounding of the Atmosphere from Low Earth Orbit: Preliminary Results; *Bulletin of the American Meteorological Society, 77*(1), 19-40, 1996.

Weng Cho Chew, *Waves and fields in inhomogeneous media*, New-York, IEEE press, 1994, 762 pp.

Zou, X., I. M. Navon, and F. X. LeDimet: An Optimal Nudging Data Assimilation Scheme Using Parameter Estimation; *Q. J. R. Meteor. Soc., 118*, 1163-1186, 1992.

Zou, X., Y.-H. Kuo, and Y.-R. Guo: Assimilation of Atmospheric Radio Refractivity Using a Nonhydrostatic Adjoint Model; *Monthly Weather Review, 123*, 2229-2249, 1995.

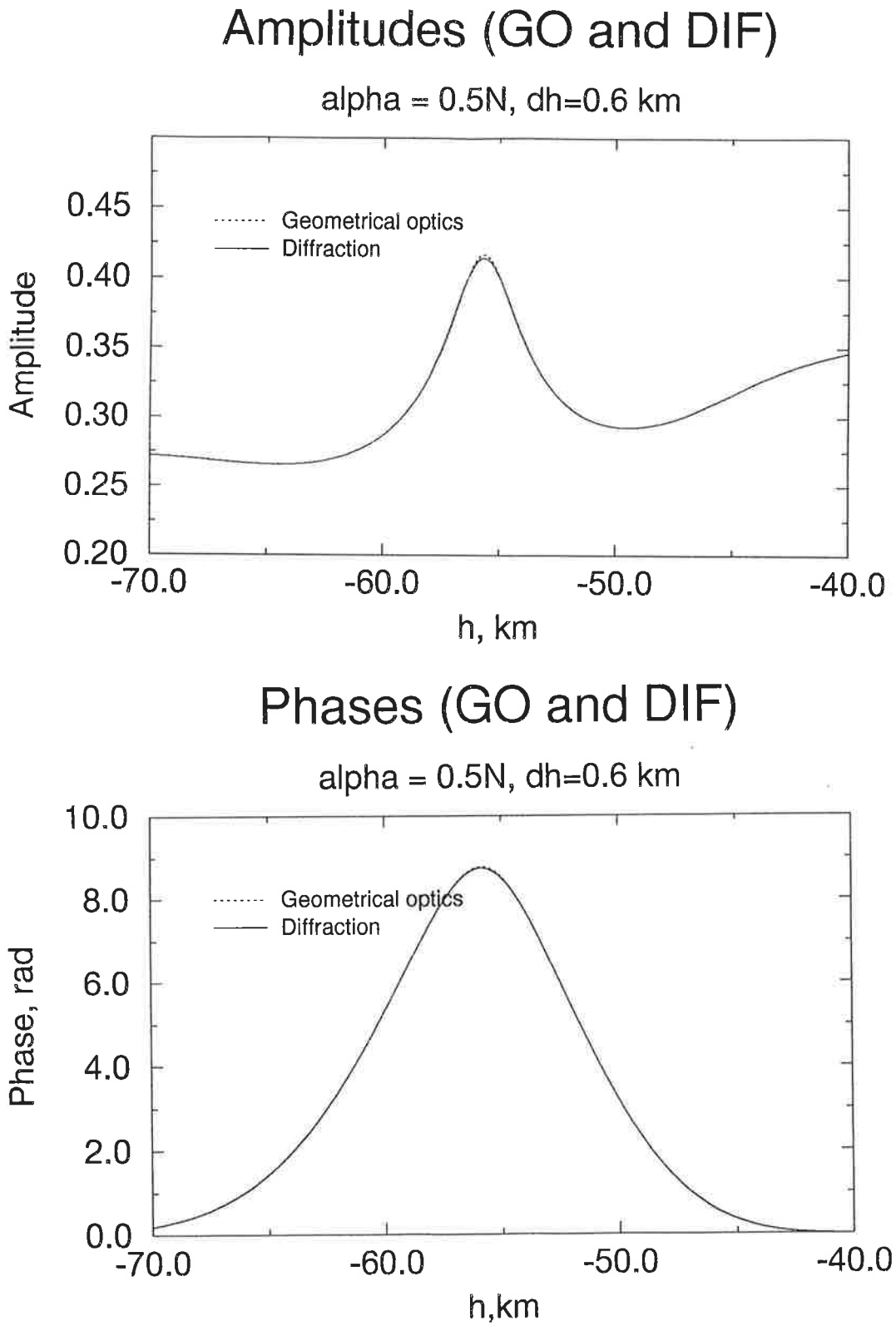

Figure 1. Comparison of geometric optical (GO) and diffraction (DIF) amplitude and phase in the observation plane. Perturbation parameters: α=0.5N, Δh=0.6 km. The size of the Fresnel zone is greater than that of the perturbation. The difference between geometrical optics and diffraction theory is insignificant.

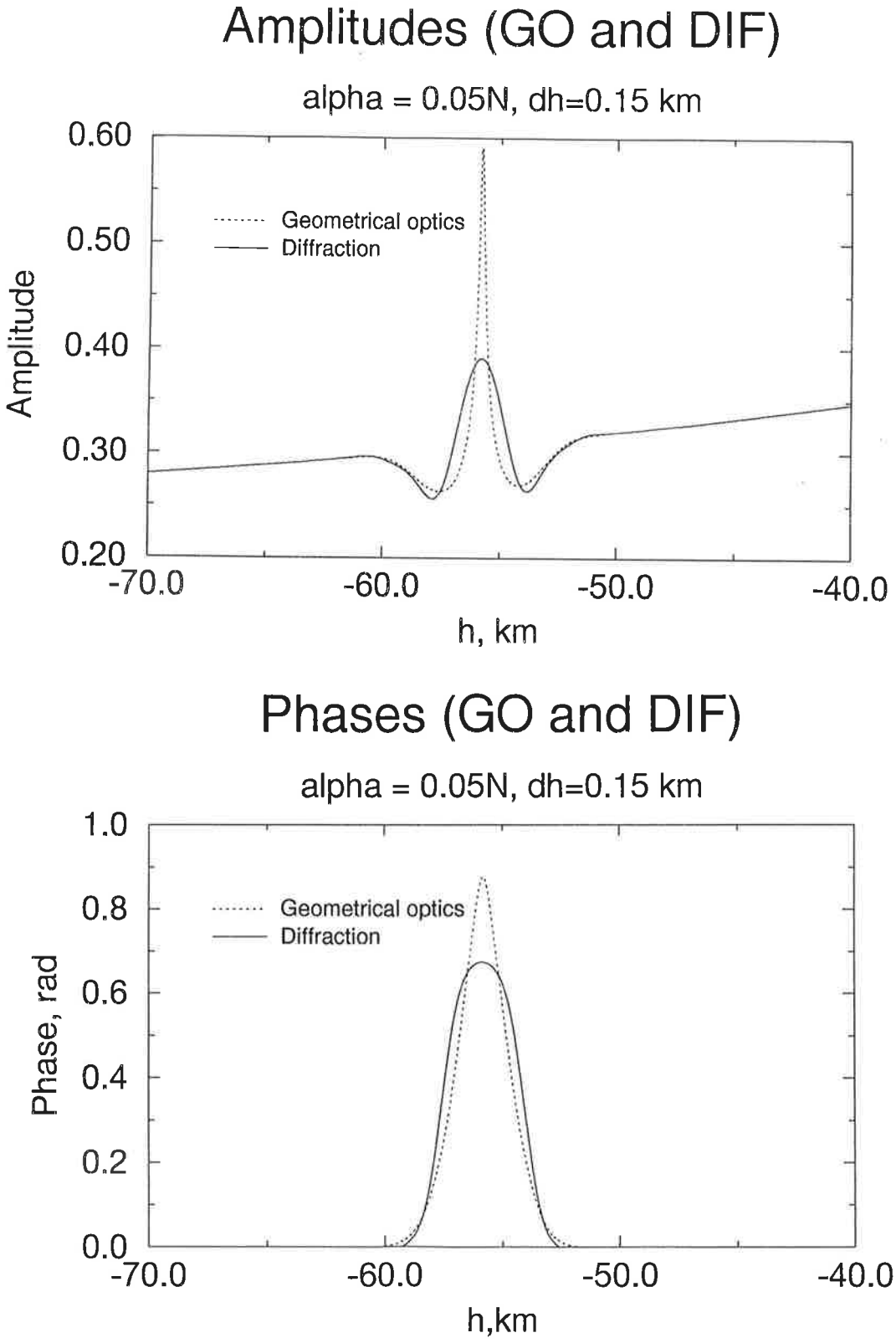

Figure 2. Comparison of geometric optical (GO) and diffraction (DIF) amplitude and phase in the observation plane. Perturbation parameters: α=0.05N, Δh=0.15 km. The size of the Fresnel zone is less than that of the perturbation. The geometrical optics predicts a much sharper focusing than the diffraction theory does.

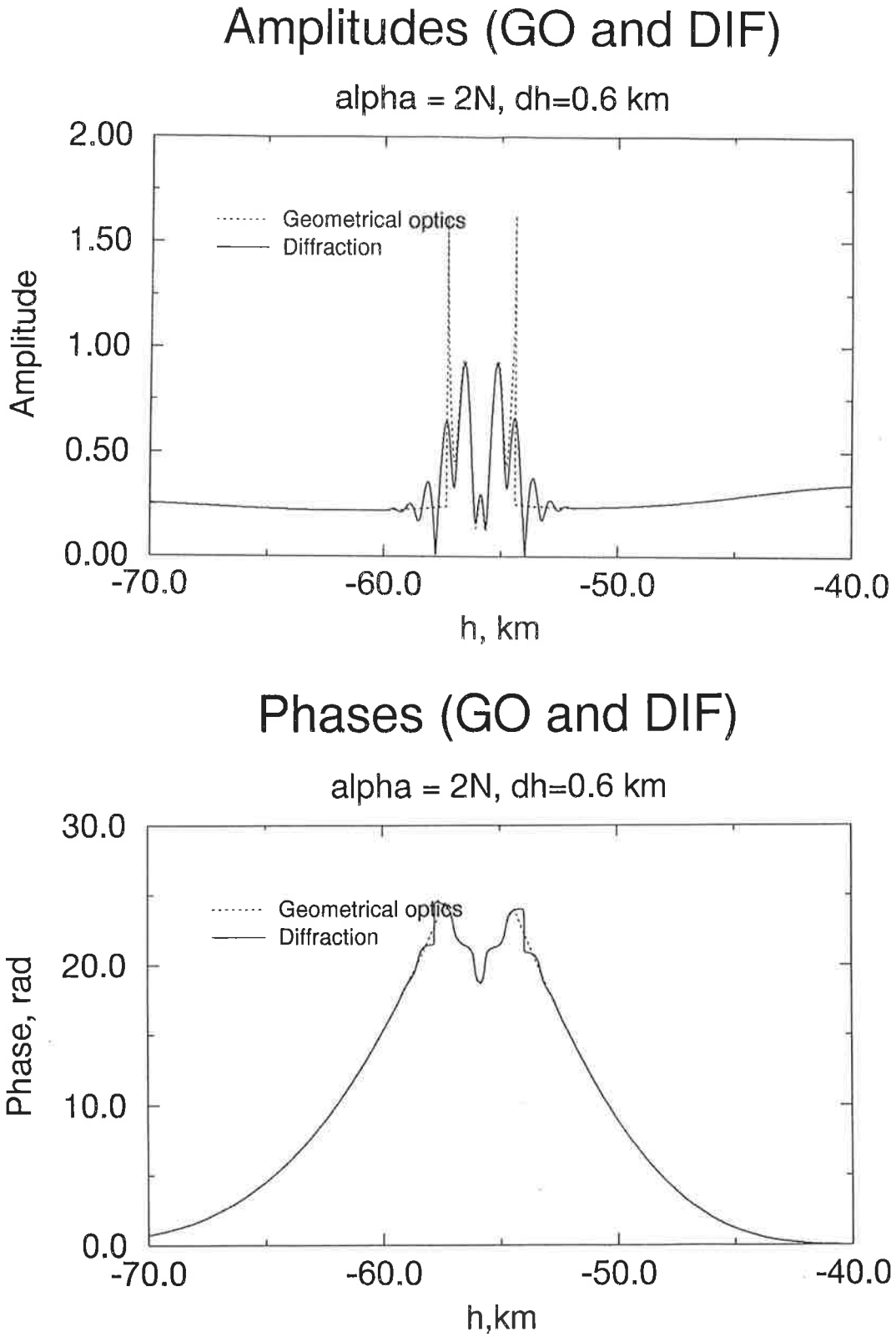

Figure 3. Comparison of geometric optical (GO) and diffraction (DIF) amplitude and phase in the observation plane in presence of multipath propagation. Perturbation parameters: α=2N, Δh=0.6 km. Visible differences between GO and DIF fields only arise in the vicinity of the caustic.

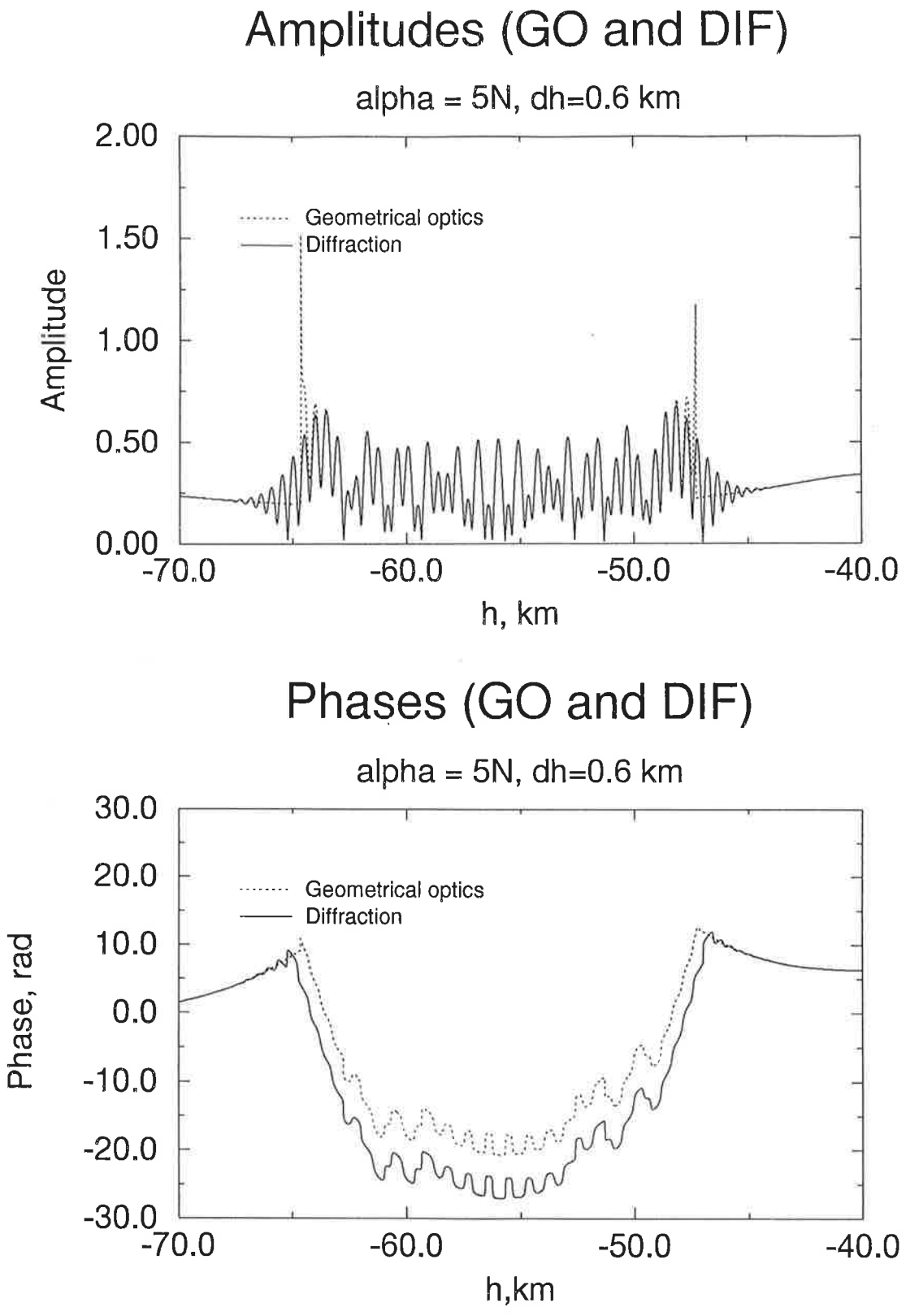

Figure 4. Comparison of geometric optical (GO) and diffraction (DIF) amplitude and phase in the observation plane in presence of multipath propagation. Perturbation parameters: α=5N, Δh=0.6 km. Visible differences between GO and DIF fields only arise in the vicinity of the caustic. The difference of the accumulated phases in the multipath area is 2π.

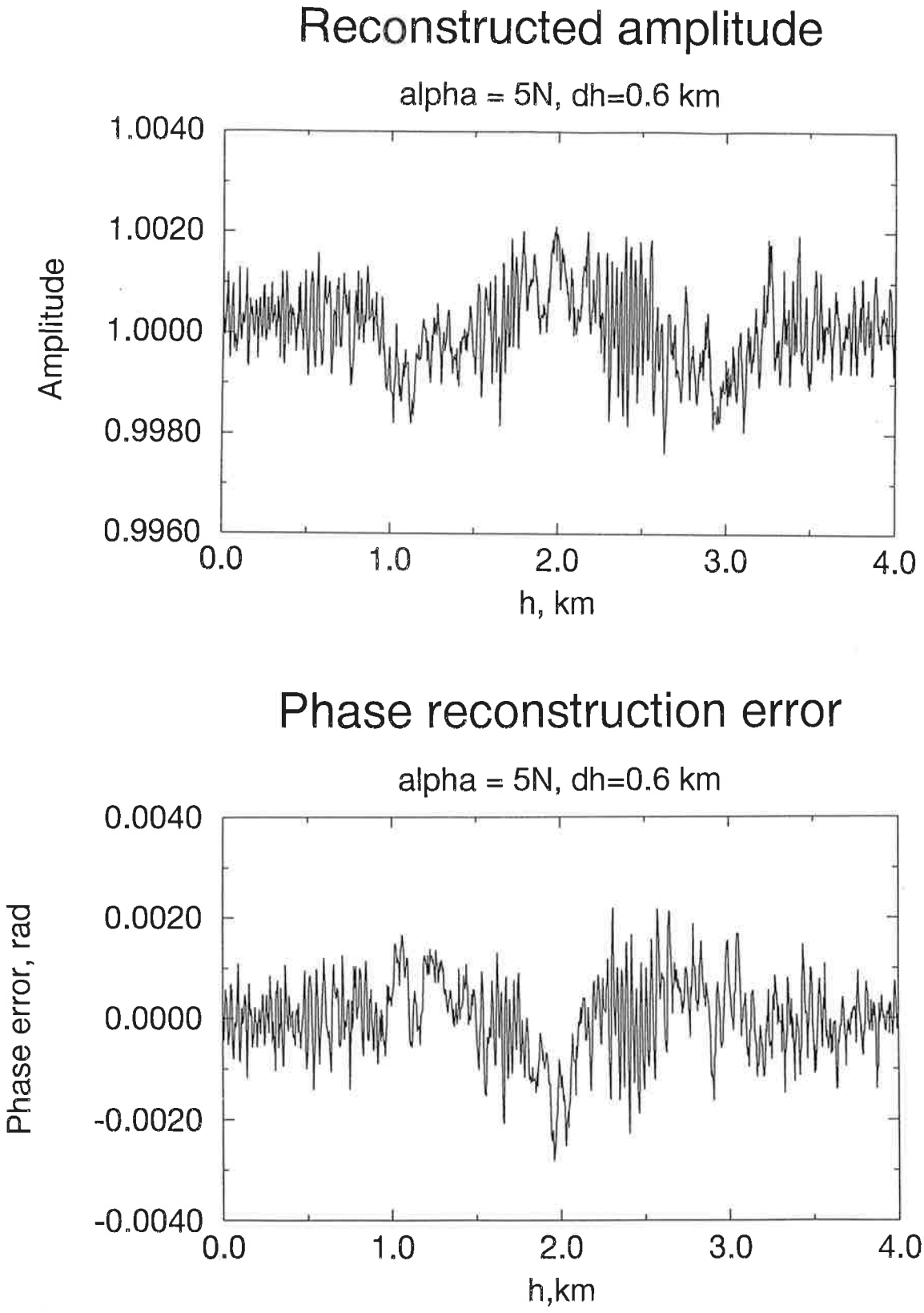

Figure 5. Reconstruction of amplitude and phase in the the thin screen plane from the field in the observation plane without measurement noise. Perturbation parameters: α=5N, Δh=0.6 km.

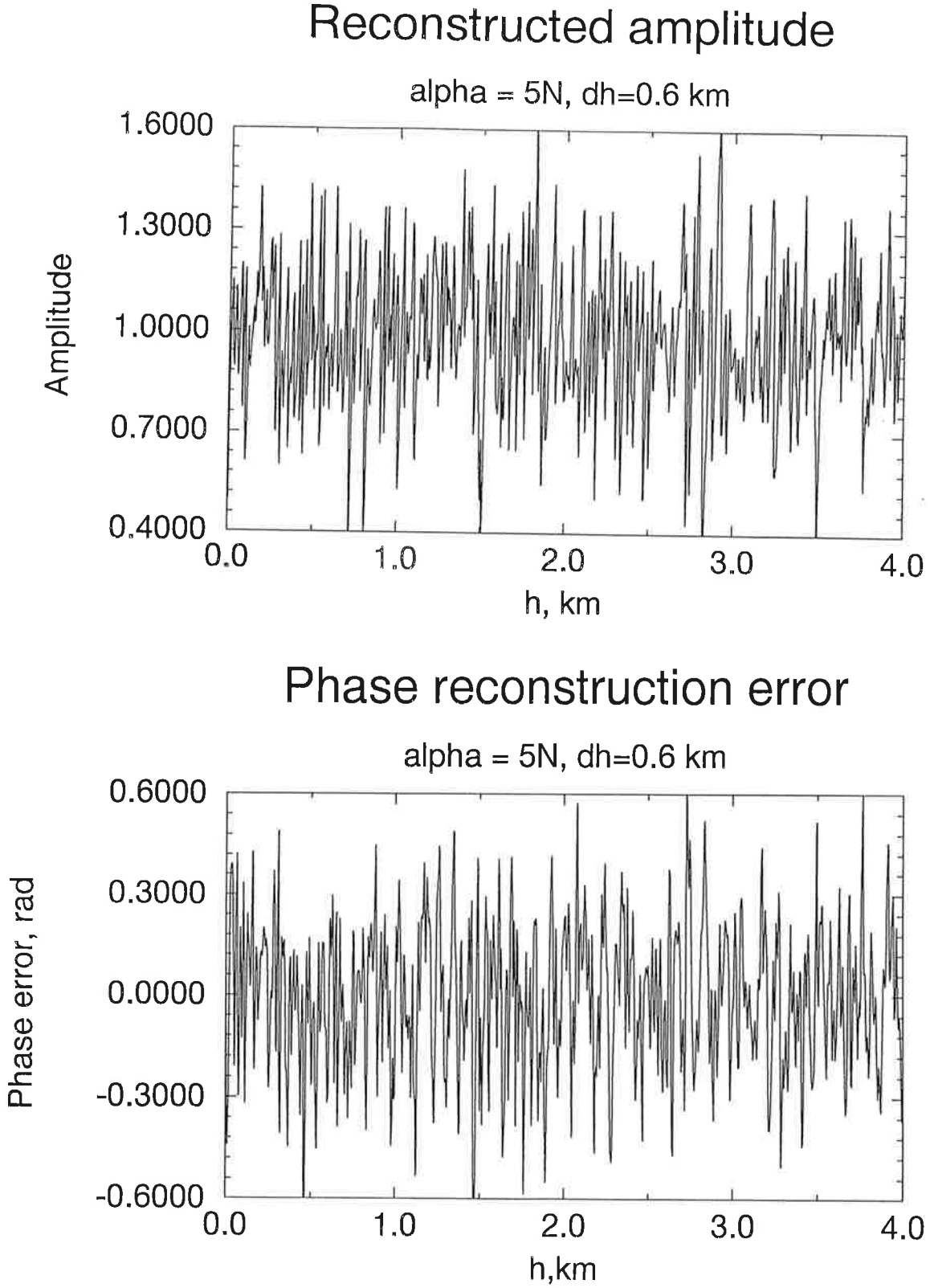

Figure 6. Reconstruction of amplitude and phase in the the thin screen plane from the field in the observation plane with measurement noise. Perturbation parameters: α=5N, Δh=0.6 km.

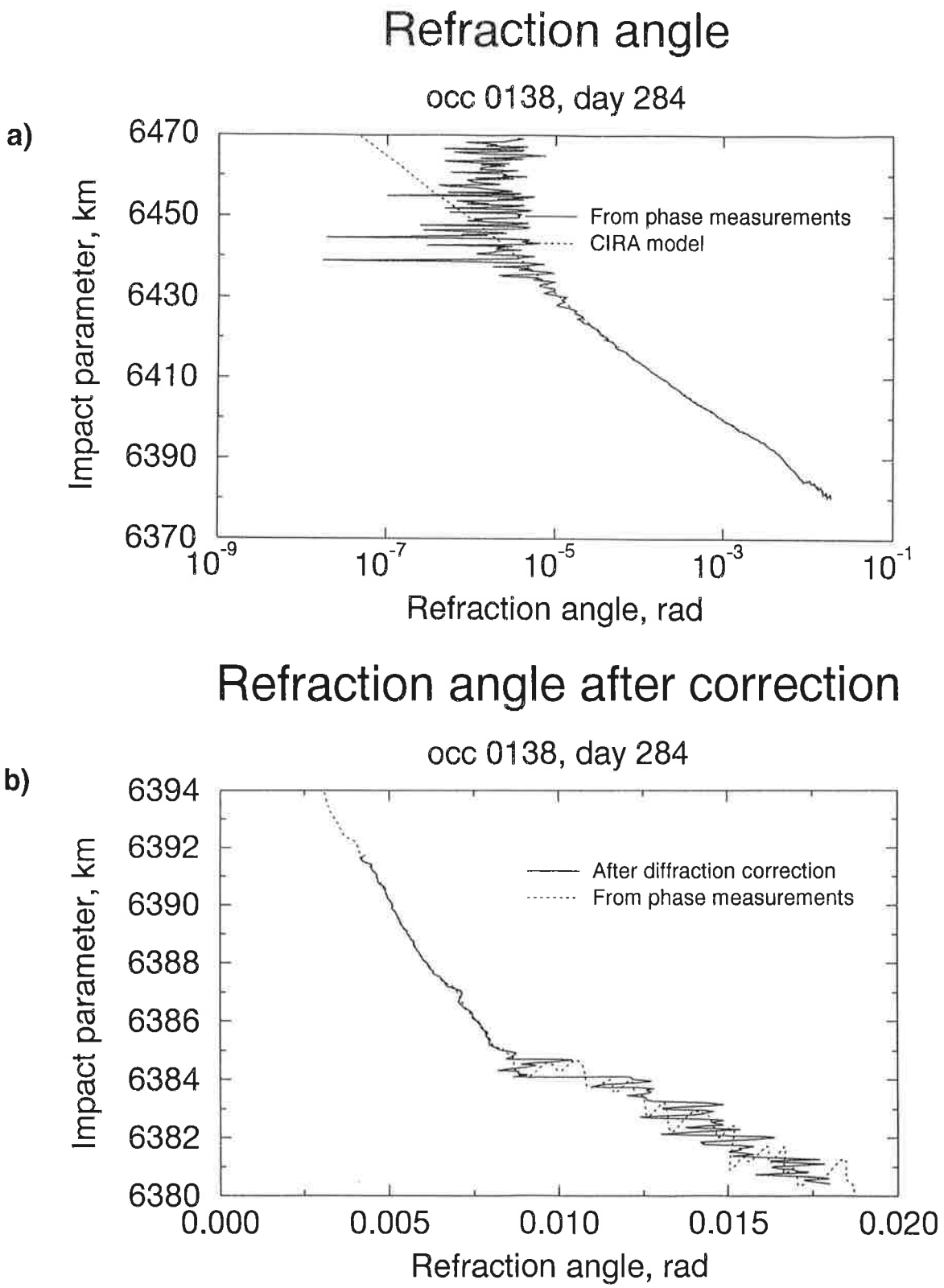

Figure 7. a) Refraction angle profiles derived from the phase measurements, calculated for CIRA model, and b) calculated after diffraction correction (occultation 0138, October 11, 1995, 16.6N 16.4W).

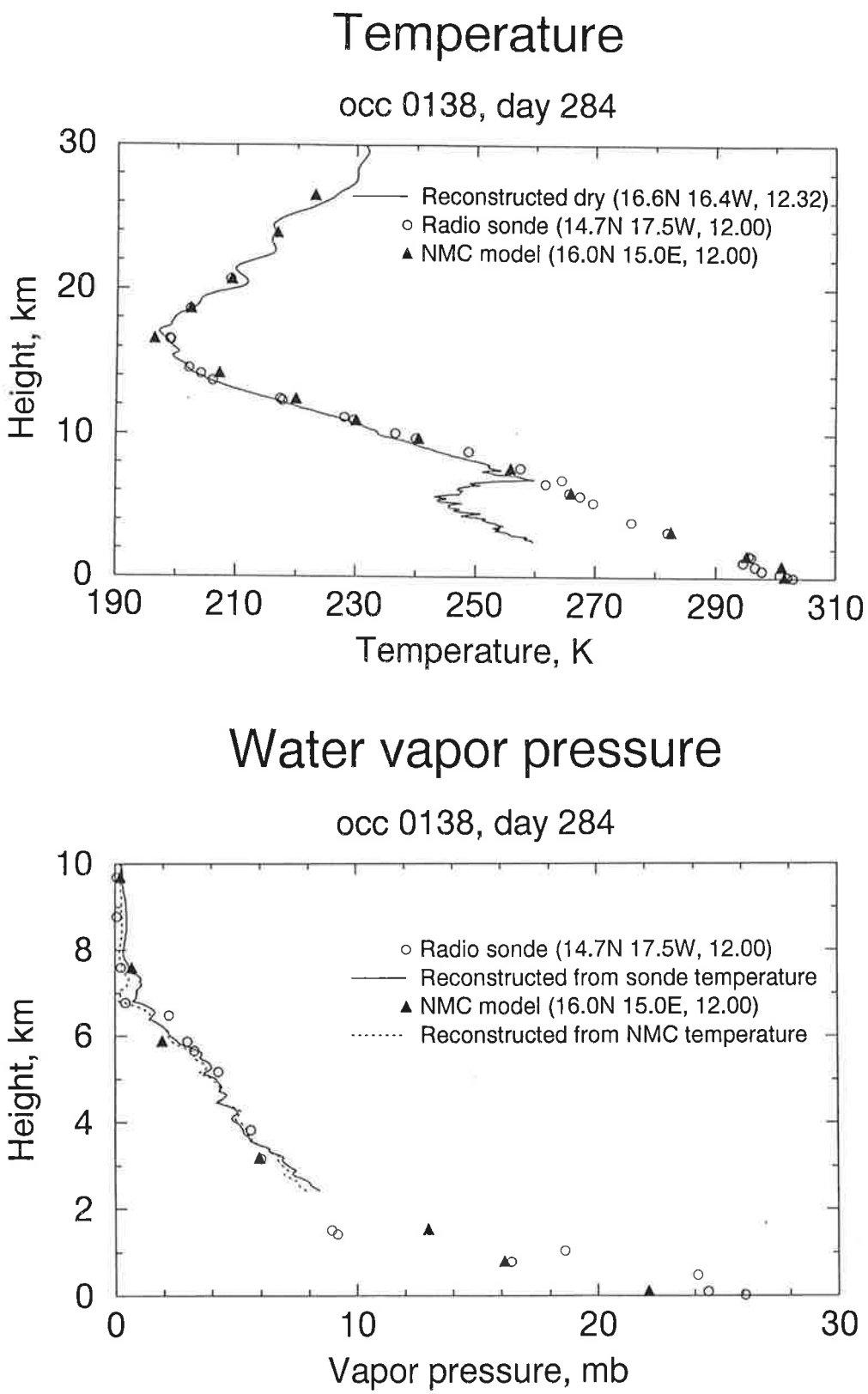

Figure 8. Reconstruction of the dry temperature and water vapor pressure (occultation 0138, October 11, 1995, 16.6N 16.4W).

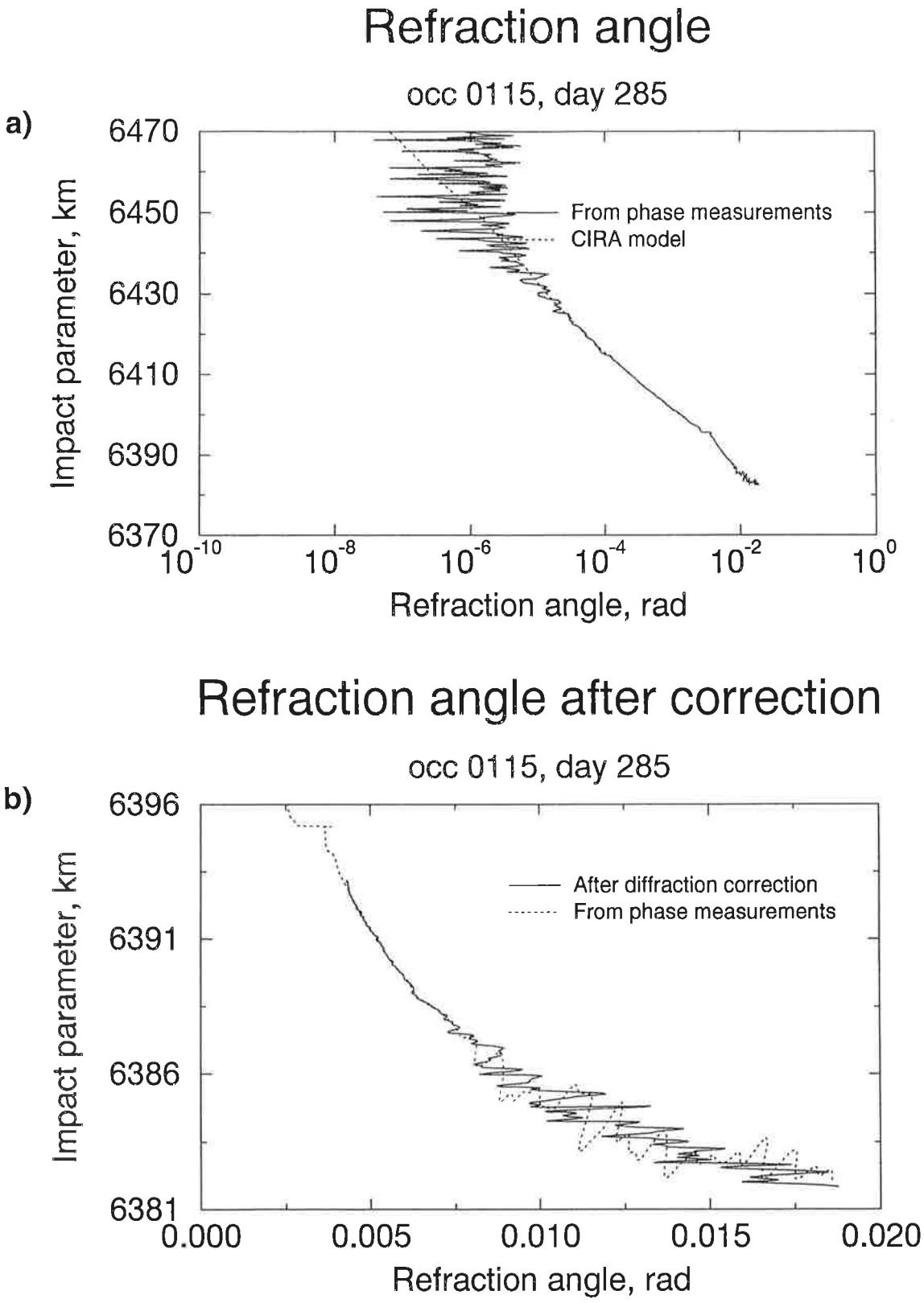

Figure 9. a) Refraction angle profiles derived from the phase measurements, calculated for CIRA model, and b) calculated after diffraction correction (occultation 0115, October 12, 1995, 1.3S 52.2W).

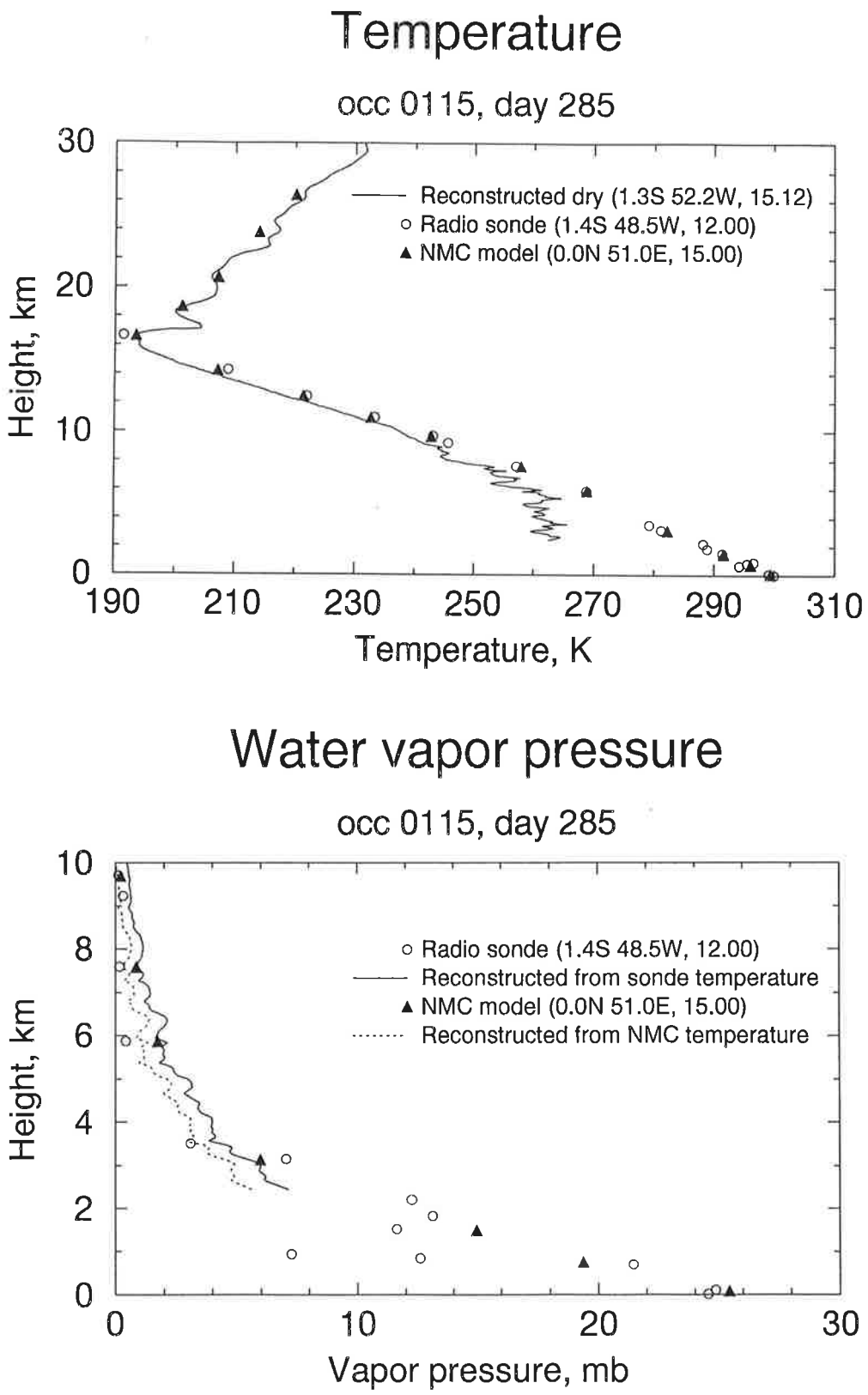

Figure 10. Reconstruction of the dry temperature and water vapor pressure (occultation 0115, October 12, 1995, 1.3S 52.2W).

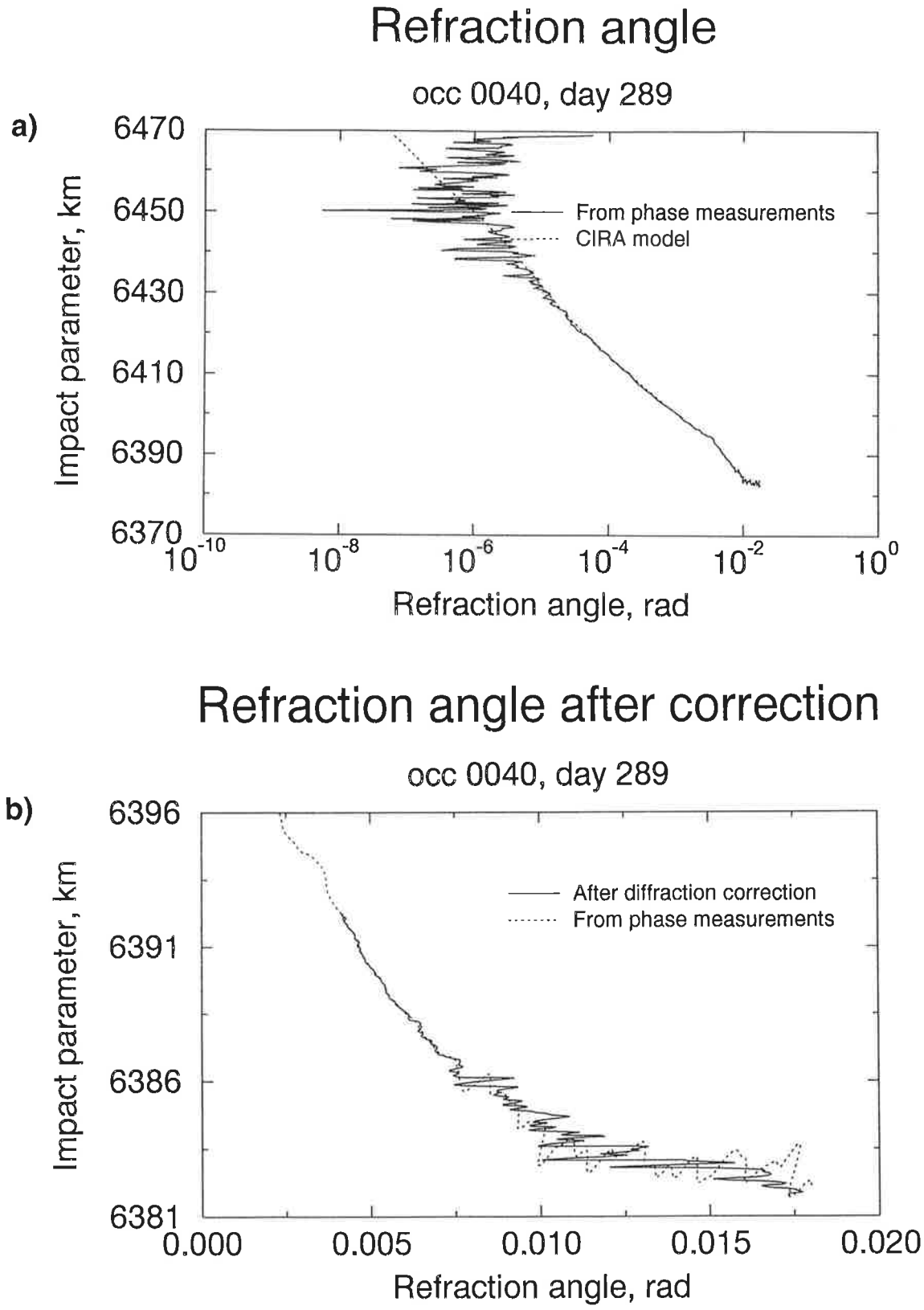

Figure 11. a) Refraction angle profiles derived from the phase measurements, calculated for CIRA model, and b) calculated after diffraction correction (occultation 0040, October 16, 1995, 12.2N 79.1E).

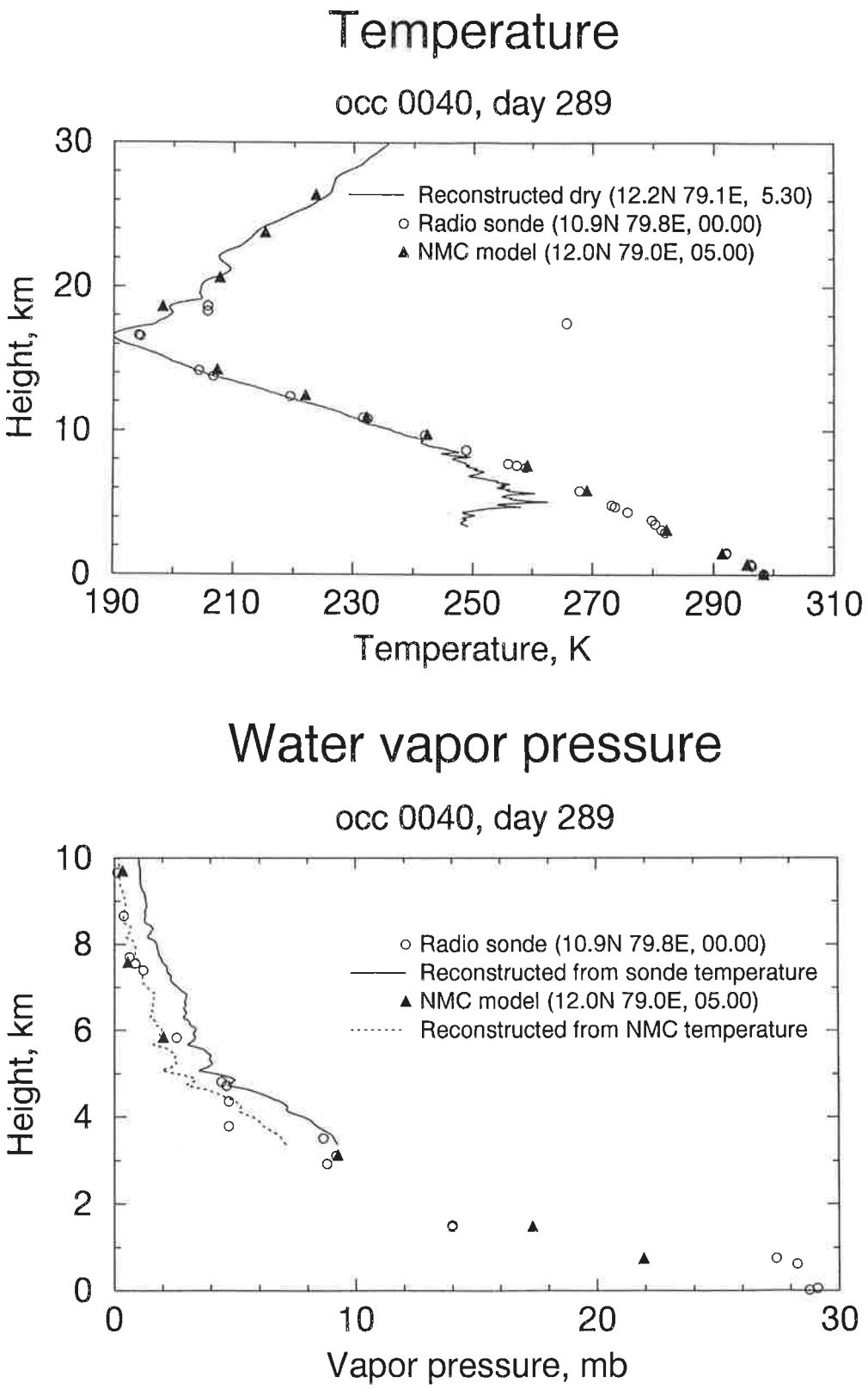

Figure 12. Reconstruction of the dry temperature and water vapor pressure (occultation 0040, October 16, 1995, 12.2N 79.1E). A large error of the radiosonde temperature at a height of 18 km is to be noticed.

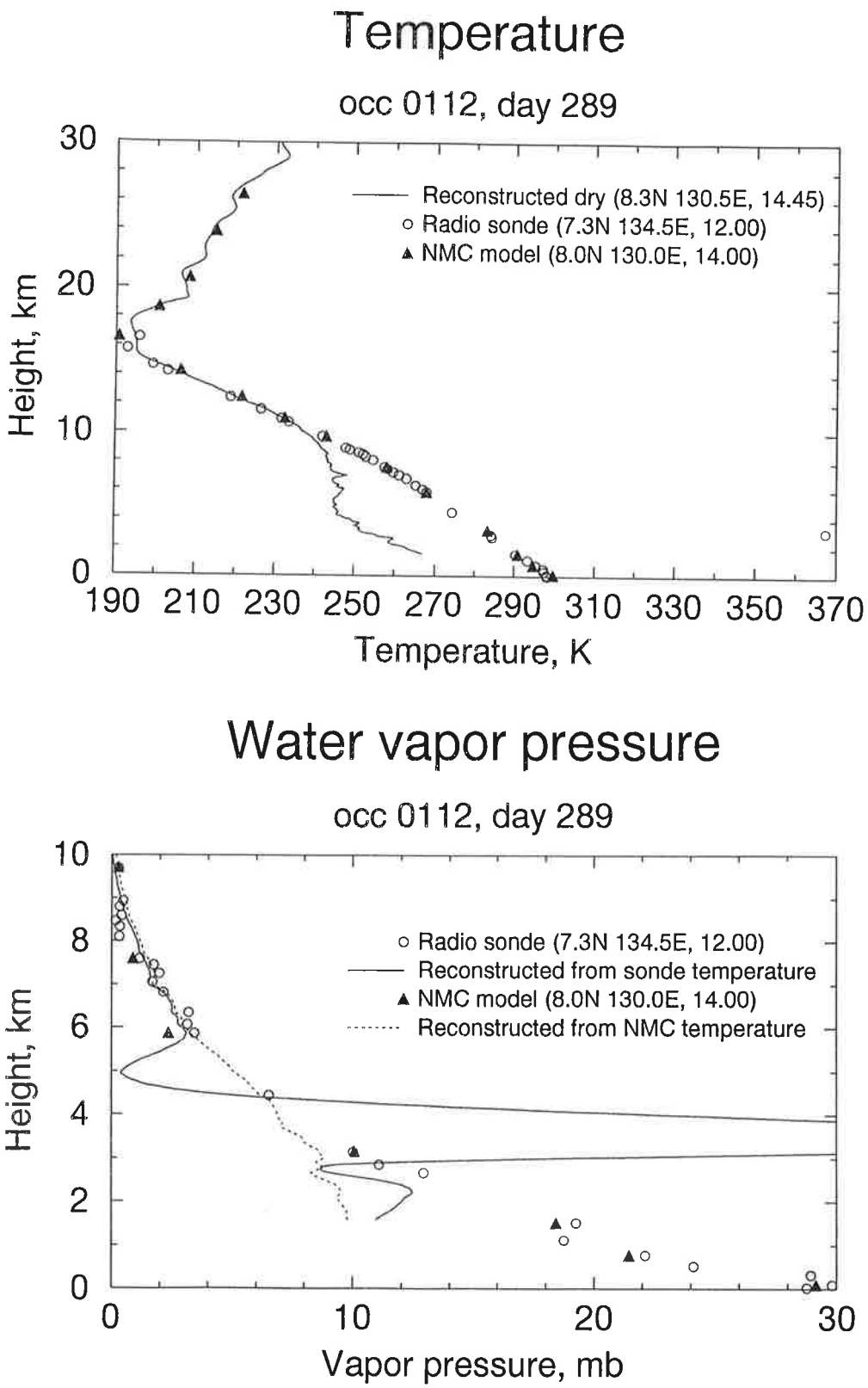

Figure 13. Reconstruction of the dry temperature and water vapor pressure (occultation 0112, October 16, 1995, 8.3N 130.5E). A large error of the radiosonde temperature at a height of 3 km is to be noticed.

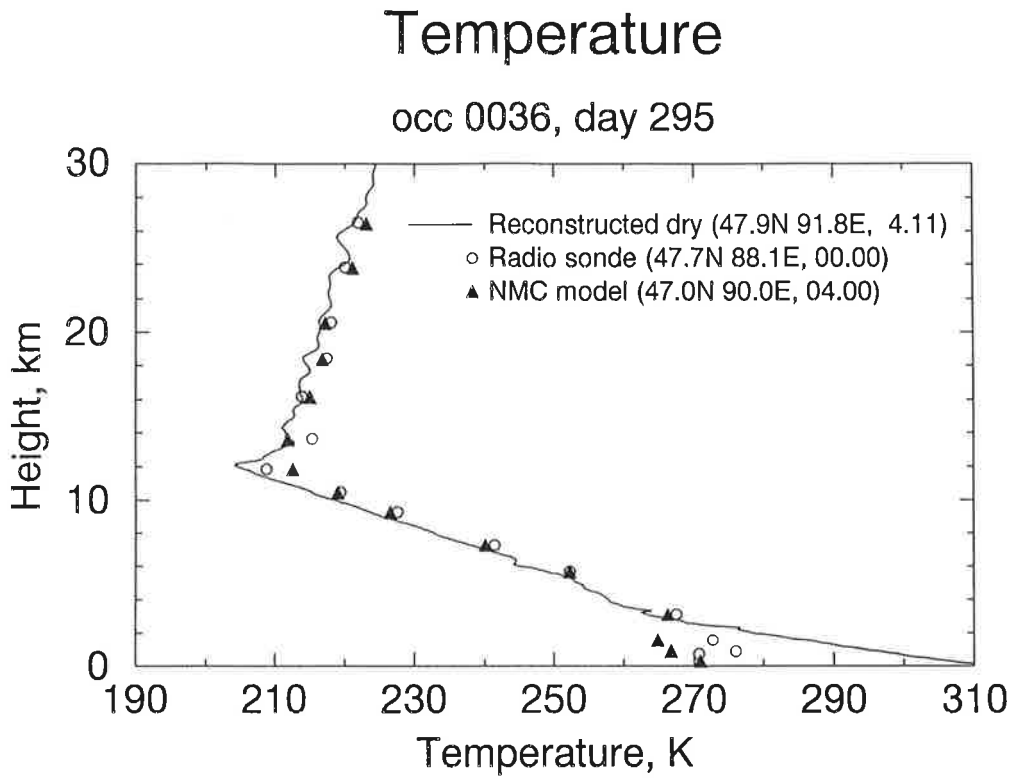

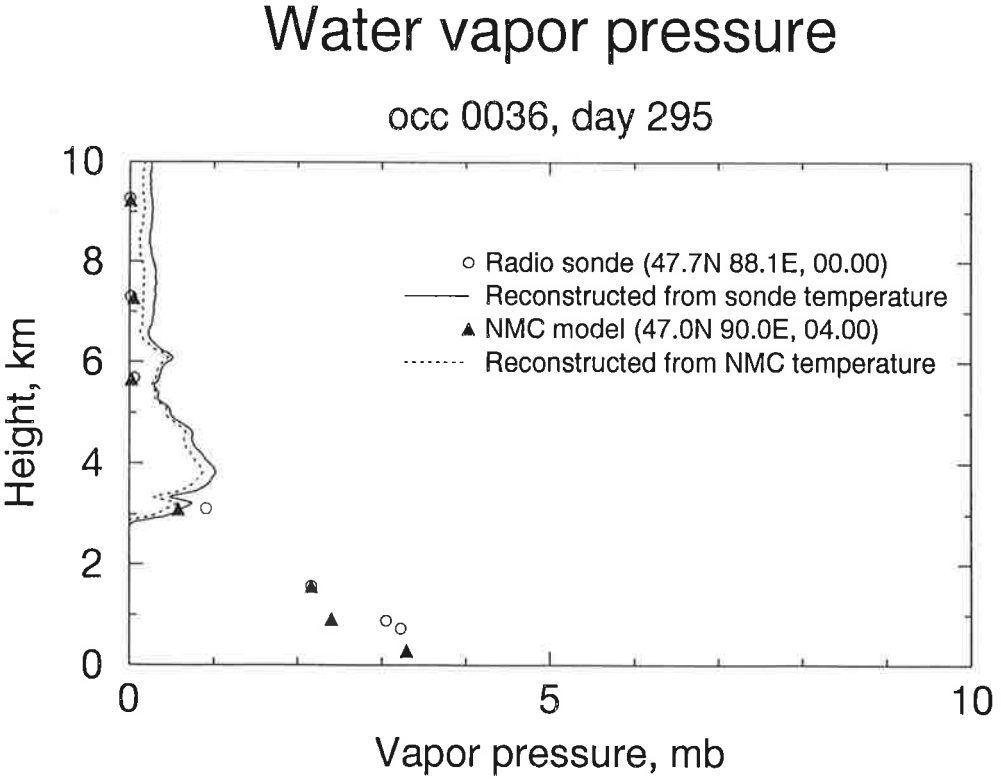

Figure 14. Reconstruction of the dry temperature and water vapor pressure (occultation 0036, October 22, 1995, 47.9N 91.8E). A tracking error of the GPS receiver in the lowest troposphere is to be noticed.

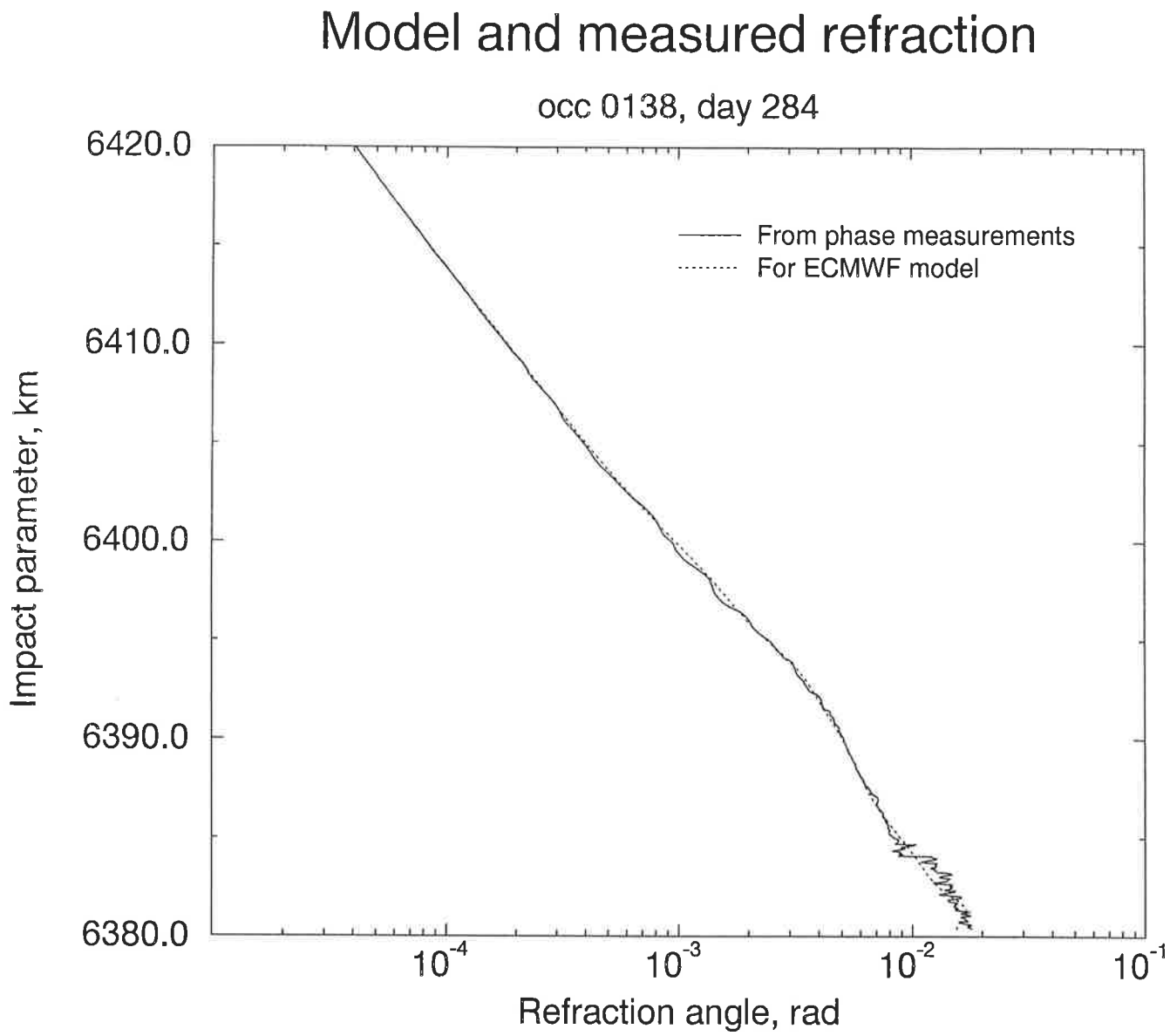

Figure 15. Refraction angle profiles: observed $\epsilon(p)$ (occultation 0138, 12.32 UTC, October 11, 1995, 16.6N 16.4W) and calculated $\epsilon_m(p)$ for the ECMWF operational numerical weather prediction model (12.00 UTC, October 11, 1995).

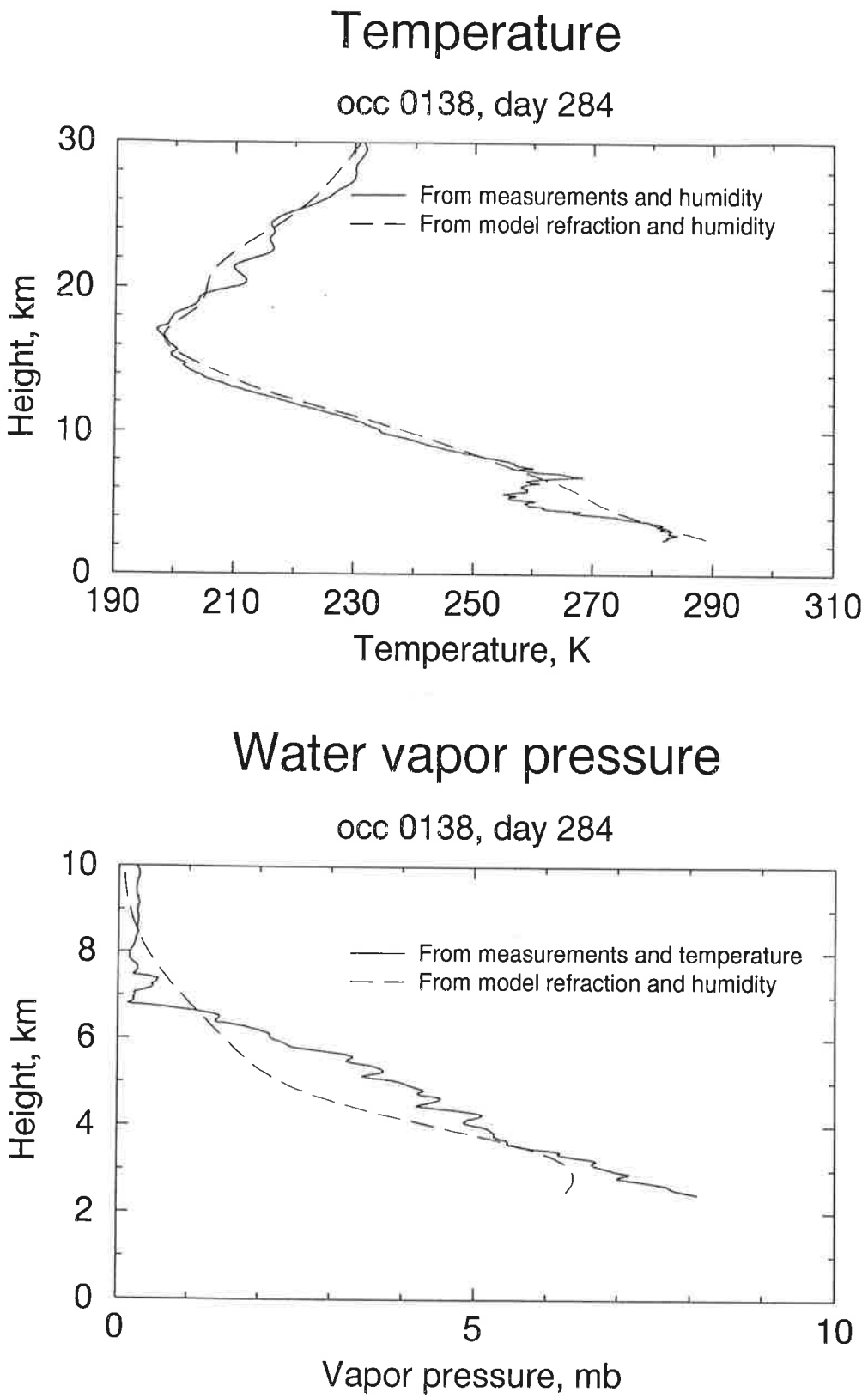

Figure 16. Temperature profiles $\widetilde{T}(z)$ and $\widetilde{T}_m(z)$, and humidity profiles $\widetilde{q}(z)$ and $\widetilde{q}_m(z)$ calculated for occultation 0138 (12.32 UTC, October 11, 1995, 16.6N 16.4W) and for the fields from the ECMWF operational numerical weather prediction model (12.00 UTC, October 11, 1995).